Review

Journal of
Nanoscience and Nanotechnology
Vol. 14, 1364–1388, 2014
www.aspbs.com/jnn

Ultrafast Laser Ablation in Liquids for Nanomaterials and Applications

S. Venugopal Rao[1,*], G. Krishna Podagatlapalli[1], and Syed Hamad[2]

[1] *Advanced Centre of Research in High Energy Materials (ACRHEM), University of Hyderabad, Hyderabad 500046, India*
[2] *School of Physics, University of Hyderabad, Hyderabad 500046, India*

We present an inclusive overview of the ultrafast ablation technique performed in liquids. Being a comparatively new method, we bring out the recent progress achieved, present the challenges ahead, and outline the future prospects for this technique. The review is conveniently divided into five parts: (a) a succinct preamble to the technique of ultrafast ablation in liquids (ULAL) is provided. A brief introduction to the conventional ns ablation is also presented for the sake of completeness (b) fundamental physical processes involved in this technique are elaborated (c) specific advantages of the technique compared to other physical and chemical methodologies are enumerated (d) applications of this technique in photonics; biomedical and explosives detection [using surface-enhanced Raman scattering (SERS)] is updated (e) future prospects describing the potential of this technique for creating unique nanoparticles (NPs) and nanostructures (NSs) for niche applications. We also discuss some of the recently reported significant results achieved in a variety of materials, especially metals, using this technique. Furthermore, we present some of our own experimental data obtained from ULAL of Ag, Cu, and Zn in a variety of liquids such as acetone, water, acetonitrile etc. The generated NPs (colloidal solutions) and NSs (on substrates) have been successfully utilized for nonlinear optical, SERS, and biomedical applications.

Keywords: Ultrafast, Ablation, Nanostructures, Nanoparticles, SERS, Nonlinear Optics.

CONTENTS

1. INTRODUCTION

Following the discovery of laser by Maiman[1] in 1960, the scientific community immediately realized the importance of lasers in science and technology, and that notion has been augmented to a great extent after the discovery of pulsed lasers. The last few decades were dedicated to the investigation of materials which enabled scientists to understand the physical, chemical, and structural properties, and utilize them for applications such as plasmonics, photonics, and biomedicine, to name a few amongst many others. The interrogation of materials in the nanoscale became an important and inevitable task since the dimensions modify basic behavior of the material via alteration of boundary conditions.[2] Ultrashort pulse interaction with materials evoked the strongest interest since their pulse duration is much less than the time required for several relaxation processes of materials viz. transfer of energy between electron and lattice systems, and heat diffusion.[3,4] These short pulse durations lead to deposition of higher energy densities (higher peak intensities) when they focus on or below a bulk target surface. Consequently, higher pressures and

*Author to whom correspondence should be addressed.

1533-4880/2014/14/1364/025 doi:10.1166/jnn.2014.9138

temperatures will be attained at the point of the impact leading to surface modification of the material and effortless fragmentation. Indeed, the transient state of the material after the irradiation of a focused, pulsed laser can be approximated by a phase transition occurring in a non-equilibrium condition[5,6] since the absorption of the high-energy density electron gas of the target material transits to a state of higher temperature via leaving the remaining target (lattice) at the initial temperatures.[7] Restoration of the system to a state of equilibrium depends on the parameters of laser pulses used for ablation and the intrinsic nature of the target. Ultrafast laser ablation (ULA) minimizes the random corrugation of the target, since the pulse duration is extremely short, and the heat-affective zone (HAZ) provided is negligible compared to the HAZ provided by the longer laser pulses. Nanomaterials have attracted the attention of the research community since they exhibit distinct indispensable novel characteristics which cannot be exhibited by conventional bulk materials.

Nanomaterials are essential building blocks of a wide range of scientific applications such as photo-induced thermal therapy,[8] biochemical sensors,[9] surface-enhanced Raman spectroscopy,[10] carriers of drug delivery,[11] nanophotonics devices,[12] in biology,[13] bio-sensing *in vivo* and *in vitro* diagnostics,[14] solar cells,[15] opto-electronic devices,[16] diabetic healing,[17] cooling systems,[18] antibacterial agents,[19] in cancer treatment,[20] in catalysis,[21] imaging, sensing, biology and medicine,[22] sensors,[23] and inkjet printers,[24] etc. We present a comprehensive overview of the ultrafast ablation technique performed in liquids. Being a comparatively new method, we bring out the recent progress achieved, present the challenges ahead, and

S. Venugopal Rao has more than 19 years of research experience in experimental Ultrafast Nonlinear Optics and Photonics. He obtained his M.S. and Ph.D. degrees from the University of Hyderabad, India. He has spent close to three years as a post-doctoral fellow with Professor Majid Ebrahim-Zadeh at the University of St. Andrews, Scotland, UK (now at ICFO, Barcelona, Spain), working in the area of Semiconductor Nonlinear Optics. From July 2003 until December 2004, he was associated with the Centre for Ion Beam Applications as a Research Fellow in the Physics department at the National University of Singapore. From December 2004 to May 2007 he was associated with the Physics department of the Indian Institute of Technology, Guwahati, as Assistant Professor. Since June 2007 he has been associated with the Advanced Centre of Research on High Energy Materials (ACRHEM), University of Hyderabad, working toward understanding the interaction of nanosecond, picosecond, and femtosecond laser pulses with high-energy materials using various time-resolved spectroscopic techniques such as laser-induced breakdown spectroscopy, ultrafast pump-probe, ultrafast ablation, and ultrafast laser direct writing. He has more than 100 papers in refereed international journals and over 150 presentations in international and national conferences. His publications have more than 1290 citations with a *h*-index of 22 in SCOPUS.

G. Krishna Podagatlapalli was born in Vijayanagaram, India. He graduated from Bhaskar Degree College, Parvathipuram in 2001. He earned his M.S. degree from Andhra University in 2004. He was with Rajah R.S.R.K. Ranga Rao College, Bobbili, teaching graduate and post-graduate students during 2004–2008. He joined for Ph.D. at ACRHEM in 2009. His research interests include ultrafast ablation, SERS, coherent anti-stokes Raman spectroscopy. He has 10 papers in refereed journals and conference proceedings.

Syed Hamad was born in Nellore, India. He graduated from Sri Padmavathi Degree College, Kavali, in 2005. He earned his M.S. degree from Sri Gayathri Vidya Parishad Degree and PG College in 2007. He was with Narayana Junior College, Nellore, teaching intermediate students during 2007–2008. He joined for Ph.D. at the School of Physics in 2009. His research interests include silicon photonics, ablation, and SERS. He has more than 10 papers in refereed journals and conference proceedings.

outline the future prospects for this technique. The review is divided into five parts:
(a) In the first part, a succinct preamble to the technique of ultrafast ablation in liquids (ULAL) is described initially. A brief introduction to the conventional ns ablation is also presented for the sake of completeness.
(b) Fundamental physical and chemical processes involved in this technique are described in the second part.
(c) Specific advantages of the technique are enumerated in the third part.
(d) Applications of this technique in photonics, biomedical, and explosives detection (using surface-enhanced Raman scattering) are presented in the fourth part.
(e) The fifth part, consisting of future prospects for this unique technique wherein a single exposure both nanoparticles (NPs) and nanostructures (NSs) are possible to fabricate.

We discuss some of the important results in a variety of materials reported recently using this technique. We also present some of our experimental results obtained from the ULAL of Ag, Cu, Al, and Zn. We utilized the generated colloidal solutions of NPs and NSs on substrates for photonic, SERS, and biomedical applications.

In this review, along with the chronicle of developments in the field of laser ablation in liquid media, we also discuss
(a) the influence of laser parameters on the products of ablation,
(b) the effect of surrounding liquid media on the ablation of metallic targets, namely Al/Ag/Cu/Zn, and
(c) the writing conditions (multiple/double/single line ablation cases) used in various experimental configurations.

2. FUNDAMENTALS OF ULTRAFAST LASER ABLATION OF SOLID TARGETS IN AQUEOUS MEDIA

2.1. Ablation of Metal in Ambient Air

Removal of a fraction of a material from the surface of a material after subjecting to strong irradiation of a focused laser beam is known as laser ablation.[25] Laser ablation of solid targets is a top-down method, and attracted the attention of the scientific community for the last half century.[26–29] The material cannot be fragmented from the surface immediate to the dumping of laser energy. The electric field provided by the impact of the laser pulse is sufficient to eject the surface electrons rather than the fragments. The ejection of electrons, ions, molecular clusters and other intermediate products are governed by two important nonlinear mechanisms viz. multi-photon absorption and cascade ionization.[30, 31] These mechanisms are purely dependent on pulse duration. Initially, surface electrons of the material absorb laser energy by means of inverse-Bremsstrahlung, and acquire higher kinetic energies. Consequently, they maintain a temperature very much higher than that of the surrounding lattice. Temperature gradient of the hot electrons and lattice can be explained by two temperature model.[32] A plasma plume[7] will be generated in the process. In general, for ultrafast laser ablation temperature of the plasma plume, pressures are $\sim 10^3$ K, $\sim 10^{10}$–10^9 Pa, respectively.[33–36] The hot electrons in the conduction band transfer the excess heat energy through the electron lattice collisions, which lasts for a few ps.[6, 25] Post thermalization, the entire system reaches an equilibrium state. At this stage, if the attained temperature is greater than melting the threshold of the material, then immediately the material in the vicinity of the impact of the laser beam starts melting. The entire process lasts for several ps. In a time scale of few microseconds, NPs are ejected from the target surface. A few articles[37–41] are reported in recent literature which discuss in detail the complete mechanisms of ultrafast ablation in ambient air. The dynamics of a target ablation even in ambient air are, to a great extent, affected by the input laser parameters. Lorazo et al.[37] had reported that pulse duration is indeed an important parameter producing different outcomes in the case of longer pulses compared to the ultrashort pulses. They have observed that isochoric heating and rapid adiabatic expansion of the material (silicon in their case) provided a natural pathway for phase explosion. This was not observed with slower, non-adiabatic cooling with ps pulses where fragmentation of the hot metallic fluid was the only pertinent ablation mechanism.[37] Amoruso et al.[38] reported the ultrafast ablation in vacuum, and comparison was furnished between the picosecond (ps) and femtosecond (fs) regime dynamics of ablation. Lorazo et al.[39] made an attempt to explain the thermodynamic pathways of the various stages of ablation in an extensive manner. Similarly, Balling et al.[40] reported the dynamics of ns laser ablation of dielectrics in air ambient with plausible explanation. Semaltianos et al.[41] reported the effect of medium (both air and liquid) on the fabricated NPs and underlying physics elaborately. Though there are many reports describing ULAL, there are not many reviews on this subject.

2.2. Ablation of Metal in Aqueous Media

If the target is surrounded by an aqueous media[42–55] then the dynamics of ablation happen to be extremely complicated. Laser ablation of metal targets in liquid (shown in Fig. 1) is a simple technique compared to the other physical and chemical methods for fabrication of nanomaterials.[56–60] When the laser beam is focused on the surface of a target material under the liquid layer, local melting of the metal target takes place. As a result, the metal portion at which the laser beam is impinged goes to melt phase. The adjacent liquid layer of metallic melt absorbs part of the heat energy and attains a higher temperature. At this temperature liquid cannot sustain in its own phase and, therefore, it expands via evaporation. During the process of evaporation the liquid layer exerts a recoil

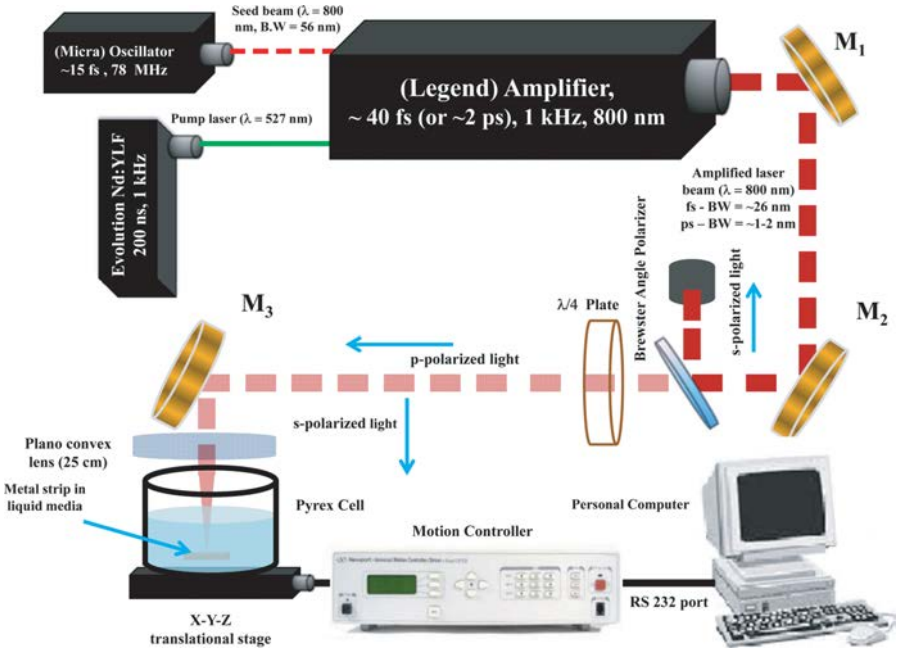

Figure 1. Experimental schematic of ultrafast laser ablation of metals immersed in aqueous media.

pressure[42] on the underlying melt. This pressure is much greater than atmospheric pressure. However, surface tension forces in the melt try to sustain as a spherical entity. As a result of the higher recoil pressures exerted by the evaporating liquid layer, metallic melt splashes into fragments, and each fragment of nanodimension goes into the surrounding liquid medium. In addition to the fabrication of NPs, redistribution of metallic melt takes place before its condensation which form different NSs.

2.2.1. Formation of Cavitation Bubble and Relative Dynamics

The physical processes, including the generation, transformation, and condensation plasma plume induced at the time of laser ablation in liquids have been investigated by many groups.[61–65] Exact dynamics of LAL are still being debated, but according to some of the recent works it is explained as a complicated laser-matter interaction under the liquid layer leading to the generation of a plasma plume. Later on, plasma expands into the surrounding liquid medium, and results in generation of a shock-wave. During the process of expansion, the plasma plume cools down and plasma transfers energy to the surrounding liquid medium. The annihilation of the plasma plume occurs in typical time scales of 10^{-8}–10^{-7} s,[66] resulting in the formation of a cavitation, which tries to expand in the medium in a time scale of 10^{-7}–10^{-6} s and continues expanding up to $\sim 10^{-4}$ s.[67] After a certain period of time (usually of the orders of few hundred microseconds) at which the inside pressure decreases compared to the surrounding liquid medium, cavitation bubble collapse takes place along with the generation of a second shock wave.[68]

The exact stage of nanomaterials production IS still under investigation. Many reports suggest that the nanomaterials are formed during the expansion of the cavitation bubble inside it on a time scale of $\sim 10^{-6}$ to 10^{-4} seconds. The expansion of the cavitation bubble into the liquid medium exerts a recoil pressure on the metallic melt formed under the plasma plume. Recoil pressure splashes the melt and residual recoil pressure redistributes the metallic melt. As mentioned above, expansion of a plasma plume and its transient dynamics can prompt the mixing of vaporized material with the liquid medium surrounding it.[69–71] Later, the vaporized material condenses into the liquid medium, resulting in solidification (generation of NPs) in time scale of few hundred ns [$\ll$time taken for condensation of vapor plume in liquid (~ 100 μs)].[72–74] Nanoentities inside the cavitation bubble are at a higher temperature than the surrounding liquid environment. The gradient in temperature on both sides of the liquid-bubble interface leads to nucleation and condensation of the fabricated nanomaterials after collapse of the cavitation bubble. The product of ablation plume may be atoms, molecules, and clusters of atoms and molecules in their charged form. Fabrication of nanomaterials not only depends on the laser parameters and material, but also on the nature of the surrounding liquid. Polarity, viscosity, and refractive index of the medium play a key role in the post ablation process such as agglomeration and aggregation. In general, ablation of metals in polar liquids results in the fabrication of NPs with smaller size through the formation of electrical

double layers (EDL) on the produced charged nanoparticle surface, which neutralizes any further aggregation. Viscosity of the liquid medium sustains the plume for a longer time, and enhances the probability of the second ablation at the point of plume formation.

ULAL is an advantageous method compared to the other well-known methods used to produce nanomaterials such as flame metal combustion,[75] chemical reduction,[76] photoreduction,[77] electrochemical reduction,[78] solvothermal,[79] electrolysis,[80] green method,[81] microwave-induced,[82] sonoelctrochemical,[83] aerosol flow reactor,[84] photochemical reduction,[85] chemical fluid deposition,[86] spray pyrolysis,[87] and spark discharge.[88] First, pulsed laser ablation in liquids avoids the contamination of the surrounding air media since the ablated fragments (NPs) from the target surface directly enters the surrounding liquid medium to form a colloidal solution. Second, usage of surfactants is not necessary to produce dispersed NPs, unlike chemical methods of nanoparticle synthesis. Third, simultaneous preparation of nanoparticle and NSs can be performed in a single experiment within in a few minutes, while generating NSs over an area of a few inches. Moreover, the fabricated NPs and NSs can be utilized for other experimental purposes devoid of subjecting them to a rigorous cleaning with chemicals. ULAL is a simple platform to produce not only the NPs of metals, but also the NPs of semiconductors,[89–90] alloys,[91] oxides,[92] magnetic materials,[93] biaxial hetero structures,[94] and core–shell type,[95] etc.

2.2.2. Parameters of Ablation

The products of ablation simultaneously depend on many parameters of the input laser pulses as well as the surrounding liquid media. Wavelength, pulse duration, fluence, beam waist, repetition rate, and number of pulses incident per unit area are the laser parameters that can affect the products of ablation. Linear refractive index and viscosity and the polarity of the liquid, along with the thickness of the liquid layer on the target surface, are liquid parameters that influence the process of ablation to a great extant. Even the variation of one of the parameters to a slight degree also affects the nature of the products.

2.2.2.1. Effect of Wavelength. Laser wavelength of the incident laser beam determines the skin depth, and as a consequence, ablation depth can be altered. Nichols et al.[96] reported that absorption of UV photons by the surface electrons via inter-band transitions was more uniform and leads to nice corrugation on the surface, whereas near-infrared radiation is preferentially absorbed by the defects and impurities of the material, consequently resulting in the formation of random surface structures. For UV radiation, the tendency of scattering is higher compared to NIR radiation. Furthermore, wavelength of the laser beam should be chosen in such a way that it must not be absorbed by the fabricated intermediate NPs within the liquid. It has been proven that incident laser wavelength should not be equal to the wavelength corresponding to the SPR peak of the NP colloidal solution, to avoid the ambiguity of intermediate absorption of incident light. If the absorption occurs, nanomaterials are subject to the modification in an unusual manner beyond certain predictions.[97–100] It has also been documented that the shorter the wavelength, the higher the photon energies through which bond breaking and ionization processes become simpler when compared to longer wavelengths.

Mortazavi et al.[101] reported the observed variations in the size distribution of the fabricated Pd NPs in de-ionized water fabricated with the wavelengths 1064 nm (Nd:YAG) and 193 nm (Excimer laser) at equal pulse durations of 6 ns. According to their data and analysis, laser ablation with longer wavelengths followed bottom-up behavior, which supported the aggregation of synthesized NPs due to thermal effects from plasma-induced ablation ending up with NPs of larger sizes. Laser ablation with shorter wavelengths follows top-down behavior, directly fabricating smaller NPs, since the photon energy is higher. Schwenke et al.[102] also reported the effect of laser ablation of metal in the solvent tetrahydrofuran with fundamental (1064 nm) and second harmonic (532 nm) in ps regime, and observed a good rate and yield of NP fabrication with 1064 nm. A linear dependence of decrease in the hydrodynamic particle size in the case of 1064 nm ablation was observed, since absorption and scattering loss is weak at this wavelength. In the case of 532 nm, ablation exponential decrement of the hydrodynamic particle size could be assigned to particle fragmentation during the post irradiation of dispersed nanoparticles. Moreover, depending on the wavelength of the incident, laser cross-section of inverse Bremsstrahlung varies and cascade ionization will be altered, since the above-mentioned cross-section directly varies with the second power of the incident laser.[25, 30]

2.2.2.2. Pulse Duration. Developments in achieving superior pulsed laser systems from ns time scales to fs time scales have further established the practical applications resulting from the advantages of pulsed laser ablation. Since the short pulsed lasers support the higher peak intensities, explosive boiling of the material under consideration became an easy task. When laser pulses of longer duration (μs to ns) are incident on the metallic targets, after the electron-lattice collisions, the thermal processes like explosive boiling[103, 104] and evaporation take place. Further, to the absorption of laser pulse, heat diffuses into the lattice from the electrons in a very short time compared to its pulse duration (μs or ns). When the laser power density is higher than the threshold of the melting energy of the material, rather than evaporation accumulated, heat energy transits the metal to a super-heated liquid state. When the surface region is heated beyond thermodynamic stability, the surface undergoes a transition from a superheated liquid phase to vapor and liquid droplets leading to the fabrication of nanomaterials. The process of ablation of targets with microsecond or ns pulses is dominated by heat conduction, melting, evaporation, and plasma formation.

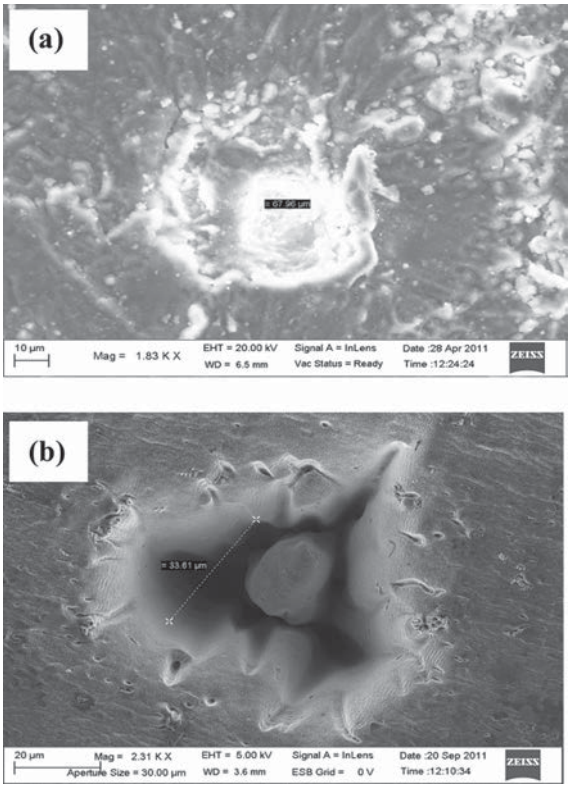

Figure 2. FESEM images of the laser-exposed portions of Al substrate immersed in water with (a) 7 ns (b) 40 fs laser pulses.

Figure 1 shows the schematic of a typical ultrafast laser ablation in liquids experimental set up. For the longer pulse, ablation heat-affected zones (HAZ)[105] prevail than for the short pulse ablation. Differences between the ablation of Aluminum by ∼7 ns, and ∼40 fs laser pulses in water are depicted in Figure 2. The melting continued for a long time resulting in the boundaries of the ablated zone does not provide sharp boundaries. In addition, a plasma shielding effect[106, 107] prevails in which the trailing part of the laser pulse suffers an interaction with the plasma generated by the leading part of the pulse, resulting in unwanted modification of the nature of the nanomaterials produced up to the extant. Recently, Niu et al.[108] reported the advantage of even longer duration pulses (ms) to promote the surface reactions of metal droplets and control over the formation of diverse NSs, hollow spheres, core–shell nanospheres, hetero structures, nanocubes, and nanowires. A vast amount of experimental work has been carried out and reported on ablation using ns laser pulses.[109, 110] Liu et al.[111] have recently reported the current progress achieved with laser ablation in liquids. Only a few reports[112, 113] have incorporated/elucidated some of the ultrafast dynamics of ULAL.

In the case of ultrafast pulses, ablation dynamics are explained by multi-photon induced absorption and cascaded photo-ionization (Avalanche). Particularly, for ns ablation, instantaneous multi-photon absorption prevails while in the case of ps ablation, the produced hot electrons buildup the avalanche. In the short pulse case, since the pulse duration τ_L is much shorter than the electron-phonon equilibration time, τ_E (10^{-12}–10^{-11} s) and liquid–vapor equilibration time τ_{LV} (10^{-12}–10^{-11} s),[114, 115] non-thermal processes prevail, while in the ablation with longer pulses thermal processes usually dominate.[116] During the ablation, unwanted interaction of the pulse with the plasma plume is avoided. Ultrafast laser ablation can be considered as an isochoric process (considerable change of volume of sample does not occur), since the irradiation of the laser pulse causes local heating in a short time, and it lasts before the expansion of metal takes place. In the ultrafast ablation, acceleration of the ionized entities to enormous velocities leads to development of higher pressures and temperatures. As the interaction time is very short, material cannot evaporate continuously, but transforms to a state of overheated liquid. As result, the NSs formed on the solid targets after irradiation of an ultrafast laser pulse exhibit sharp boundaries with nice corrugation, since the material is evaporated with a minimal HAZ.[117–120]

Barmina et al.[121] performed the ablation of Tantalum (Ta_2O_5) with laser pulses of duration 350 ps, 5 ps and 180 fs, and their corresponding wavelengths were 1064 nm, 248 nm and 800 nm, respectively, for fabricating metallic nanostructured substrates. According to them, surface nanostructuring chiefly dependent on the laser pulse duration (defines the energy density) than the wavelength of incident laser. In the case of 180 fs pulses (it was not observed with the other two pulse durations), they observed small-scale periodic structures (along with hillocks) of periodicity less than the laser wavelength. Leitz et al.[122] also reported the fundamental differences between the longer pulse ablation of targets with ultrafast pulse ablation, and the effect of the number of pulses on ablation along with the spot size at the focus were discussed. Barcikowski et al.[123] demonstrated the efficiency of the ps and fs pulsed laser ablation of an Ag strip in water flow. It was observed that the ablation with liquid flow improved the reproducibility and increased the NPs productivity by 380%, compared to ablation performed with stationary liquid. Fs ablation in water was 20% more efficient than ps laser ablation, but due to higher ps laser power (higher repetition rate), the NPs productivity at the same fluence was three times higher for ps ablation. They observed that fs (120 fs, 5 kHz) ablation was efficient to generate 2 μg of NPs/Joule, where as it was 1.5 μg for ps (10 ps, 50 kHz) pulses. At the same time, the rate of generation observed was excellent for ps ablation (34 mg/h) compared to fs ablation (6 mg/h). Riabinina et al.[124] investigated the ablation in water to produce better yield gold NPs and found that 2 ps was the optimal pulse duration at 5 mJ energy per pulse, at the expense of photo-ionization. Other important works of ULAL are presented in Table I.

Table I. Summary of recent reports on ULAL.

Material	Aqueous media	Laser parameters	Avg. NPs size	Miscellaneous	Ref.
Titanium, nickel, molybdenum, tungsten	Water	Nd:YAG, 1064 nm, 350 ps, 300 Hz 248 nm, Kr, 5 ps, 10 Hz 800 nm, Ti:Sapphire, 180 fs, 1 kHz. 355 nm, Nd:YAG, 150 ps, 10 Hz.	50 nm-Ni 100 nm-Ti Mb-220 nm	NSs were formed	[138]
Gold	Water KCl NaCl NaOH propylamyne	Ti:Sapphire, 800 nm, 120 fs, 1 kHz	1–250 nm (water) 1–12 nm (NaCl) 1–15 nm (KCl) 1–18 nm (NaOH)	Fluence reduction of the Au NPs by adding NaCl or KCl	[139]
	Water	Ti:Sapphire 800 nm, 45 fs, 1 kHz		Plasma generation via heating in absorption regime, plasma generation in the near field regime	[140]
	Double-distilled water	Ti:Sapphire 800 nm, 120 fs	23 nm	Bi-conjugation	[141]
	Water + β-CD + NaCl + HCl or NaOH	Ti:Sapphire 800 nm, 110 fs, 1 kHz			[142]
	Water water + CTAB	Ti:sapphire 800 nm, 100 fs, 1 kHz	5.3 ± 2.1 (CTAB) 11.9 ± 7.8 (water)		[143]
	Water + penetratin	Ti:Sapphire 800 nm, 120 fs, 5 kHz		Conjugation	[144]
Zirconia	Water	Ti:Sapphire, 800 nm, 120 fs, 1 kHz		Raman spectra was discussed	[145]
CdSe	Methanol deionized water acetone	Ti:Sapphire, 387.5 nm, 180 fs, 1 kHz	6–11 nm	PL studies	[146]
Tantulum		(1) Nd:YAG 1.064 μm, 350 ps, rep rate 300 Hz (2) KrF LASER (248 nm) 5 ps, 10 Hz (3) Ti:Sapphire, 800 nm, 180 fs, 1 kHz	Nano-hillock drop 200–300 nm	Nano texturing of tantalum; periodic structures were also observed	[121]
Silver	Deionized water	Ti:Sapphire: 800 nm, 120 fs, 5 kHz	26 ± 10 nm	Hydrodynamic size of the particles changes during the prolonged ablation and reaches a more stable level after 400 seconds	[147]
	Water or acetone	1030 nm, <30 ps, 200 Hz			[148]
	Water + SC + PVP	Ti:Sapphire: 800 nm 80 fs, 250 Hz	2 nm (nanopores)		[149]
Ni	Ethanol	Nd:YAG, 1.064 μm 350 ps, 300 Hz	30–35 nm	SERS of BPE molecules and MB molecules	[150]
Al	Ethanol	Ti:Sapphire: 800 nm 200 fs, 1 kHz; 30 ps or 150 ps	10–60 nm		[48]
	CCl_4 and $CHCl_3$	Ti:Sapphire: 800 nm 40 fs, 1 kHz;	30 nm 15 nm	Effect of the polarity of the liquid investigated	[136]
Si	Distilled water	Nd:YAG 1064 nm 34 ps, 10 Hz	23 nm/18 nm		[151]
	Ethanol	Ti:Sapphire, 800 nm 35 fs, 1 kHz;	30–100 nm		[152]
Au	Deionized water	Ti:Sapphire: 800 nm 140 fs, 1 kHz;	55 nm	After post fragmentation size of NPs 5–20 nm (15 mint.) 11 ± 5 nm (30 mint)	[252]
Au	Polymer solution	Ti:Sapphire: 800 nm 110 fs, 1 kHz;	1–15 nm	Abundance of large NPs significantly decreased as the dextran concn. increased from 0.01 to 1 g/L.	[254]
Au	Dextran β-Cyclodextrin PEG	Ti:Sapphire: 800 nm 120 fs, 1 kHz;	2.5 nm 3.2 nm 7.7 nm	Two-step (ablation and fragmentation) water (20 ± 4 nm) dextran (3.5 ± 0.6 nm)	[255]
Au foil	Water	Ti:Sapphire, 800 nm 120 fs, 100–5000 Hz	10–100 nm	Repetition rate based hydrodynamic size control	[267]
PtIr	Acetone	Ti:Sapphire, 800 nm 120 fs, 5 kHz	63 nm (hydrodynamic) 26 nm (feret)		[268]

2.2.2.3. Energy per Pulse, Spot Size, and Fluence. In principle, the decomposition or material removal from a solid is the consequence of an energy input into the target, resulting in the domination of the target's binding energy. In ULAL the total density of hot electrons depends upon the energy of the primarily ejected ballistic electrons, since their kinetic energy only determines the number of secondary electrons. The electrons mentioned are the supreme initiators of the formation of metal melt through electron-phonon collisions to attain equilibrium. Thus, the entire phenomenon is depending on the pulse energy incident laser beam. Zhigilei et al.[125] performed molecular dynamics simulations to explain the effect of laser parameters on the ablation and its products. Their studies have revealed that the rate of ablation will be different for different pulse energies, and productivity of nanomaterials fabrication has a linear relationship with the pulse energy. At higher energies, the volume of melt reservoir will be high and, consequently, more number of particles can be fabricated. But in the sense of nanostructure fabrication, up to a certain energy corrugation was observed to be good, and beyond which corrugation became random structuring. The main reason behind this is the occurrence of many dynamics like fragmentation, phase explosion, boiling and vaporization, as explained by Zhigilei et al.[126, 127]

Similarly, laser spot diameter at the focus also play a crucial role in determination of the products of the ablation. If the beam waist lies exactly on the surface of the target, microstructures were observed; whereas the nanoripples with a periodicity of the order 400 nm were observed on the Al target when ablation was carried out with 40 fs laser pulses. At the central part of the beam waist fragmentation mechanism prevails, while at the edges thermal mechanisms prevail. Indeed, the absorbed energy density per unit time and unit volume by the material at the focal plane is related to the gradient of the pointing vector.[128] If the laser beam is very tightly focused on the target surface, it dumps the entire energy and may increase the productivity of the NPs, but simultaneously loses its control on the fabrication of structures with sharp boundaries, since tight focusing leads to a gradient of temperature and pressure and, consequently, a gradient of the pointing vector. In the case of a moderately focused laser beam, the gradient of the pressure and temperature are smoother, leading to fine ablation of the target surface with a better performance in fabrication of both NPs and NSs.

The combined effect of beam waist at the focus and energy per pulse determines the laser fluence, and this combined effect ablates the material in a different way to produce NPs and NSs. Elsayed et al.[129] also investigated the fabrication of gold NPs in water for different laser fluences using 10 ns pulses, and discussed increment and decrement about the certain fluence and sizes of the gold NPs. Along with this, ablation of the gold surface exactly at focus and just above/below the focal plane were also investigated. Kabashin et al.[130] investigated the effect of 110 fs pulses fluence in the fabrication of gold NPs in water. They observed that the yield of Au NPs were good at higher laser fluences (1000 J/cm^2), rather than at lower fluences (60 J/cm^2). Moreover, nanoparticle distribution was observed to be good at the lower fluences rather than at higher fluences. Average size was small in the former case than the latter case for Gold NPs. At intermediate fluences both smaller and larger NPs were observed. Barsch et al.[51] reported the fabrication of Ag, Cu, Mg and ZrO_2 NPs with ps laser pulses. He made an attempt to explain the fabrication of the mentioned metal and ceramic NPs at different fluences and focal positions.

2.2.2.4. Number of Pulses. One more important parameter is the number of laser pulses per spot which strongly affect the ablation outcomes of yield, size distribution of the NPs, and the structure of the metal surfaces. The threshold fluence is the function of number of pulses impinging at the point of ablation. For multi-shot ablation the threshold fluence is different from the single-shot ablation, since the incubation effects diminish the ablation threshold. In the single-shot ablation absorption of the laser energy by the target follows the Beer Lambert's relation. But in the case of multi-shot ablation we cannot apply the Beer Lambert's relation, since the reflectivity drops during the first few pulses. The efficiency of the input energy coupling with the surface structures through the established surface plasmons increases, and thereby inducing losses in reflectivity of the input beam.[131] Lietz et al.[122] discussed the effect of number laser pulses in the crater formation for microsecond, ns, ps and fs pulses, and diameter of the holes formed were increased to a greater extent and blurred in the case of micro (1000 pulses) and ns (250 pulses) ablation, to a smaller extent in the case of ps (500000 pulses) and fs (5000 pulses).

3. SIMULTANEOUS FABRICATION OF NPs AND NANOTEXTURED SURFACES

3.1. Effect of Polar and Non-Polar Liquids on the Morphology of NPs

Surrounding liquid medium shows a different effect on the fabrication of the nanomaterials compared to the ambient air. Many authors reported the effect of liquid medium on the ablation (though with ns pulses in many cases) in an extensive manner.[42–55] Barcikowski et al.[132] demonstrated the influence of the air and liquid individually on the fabricated NPs. Furthermore, the nature of the liquid medium[133] was revealed to show a great impact on the products of ablation viz. NPs and/or NSs. Sylvestre et al.[134] reported the interaction of surrounding water medium with the generated plasma to fabricate gold NPs with ns laser pulses. NPs and fabricated NSs are the result of the amount of recoil pressure of the vapor of the liquid on the melt of the metal. Accordingly, the mentioned recoil pressure depends on the latent heat of vaporization (LHV) of the liquid used. If LHV is high then it can exert a large amount of

pressure on the metal melt. During the ablation of metallic targets in the liquid environment, the molten layer borders directly on the vapor of the ambient liquid. The viscous interaction of the vapor and target surface with the molten target layer may be responsible for several instabilities, like Kelvin-Helmholtz or Rayleigh-Taylor; these instabilities might cause the fabrication of NSs on the target surface.[44] After the generation of NPs the growth and aggregation takes place under the influence of the liquid environment. The NPs growth and aggregation depends upon the permittivity and the polarity of the molecules of the surrounding liquid medium.[135] The results of ablation are different for a non-polar liquid environment compared to a polar liquid environment.

To investigate the above-mentioned effect, ablation of Al target with 40 fs laser pulses was performed by submerging it in the organic liquids carbon tetrachloride (non-polar) and chloroform (polar) at the same experimental conditions.[136] ULAL was carried out using chirped pulse amplified (CPA) Ti:Sapphire laser system (LEGEND, Coherent) delivering nearly transform-limited laser pulses (~2 ps, 1 kHz repetition rate) at 800 nm. The amplifier was seeded with ~15 fs (55 nm FWHM) pulses from an oscillator (MICRA, Coherent, 1 W average power, 80 MHz repetition rate, 800 nm central wavelength). Al substrate submerged in double-distilled water (2–3 mm above the Ag sample) in a Pyrex cell was placed on a motorized X–Y stage. Plane polarized (s-polarization) laser pulses were allowed to focus vertically onto the Ag substrate through a plano-convex lens of focal length 25 cm. The position of the focus was approximated to be at the point where plasma was generated. X–Y translation stages, interfaced to a Newport ESP 300 motion controller, were utilized to draw periodic structures on the Al substrate with a given separation. Moreover, the mentioned solvents are oxygen-free, so that they can prevent the oxidation of Al NPs and Al NSs to a reasonable extent. Analysis of the collected colloids revealed that the post-ablation process is an important factor to determine the average size and range of distribution of the fabricated Al NPs. Ablation generates the NPs, atoms, molecules, and their clusters with a residual surface charge. Consequently, these small fragments show a tendency to deposit on the surface of the NPs, as they are charged entities. If the surrounding liquid molecules are polar in nature, then these molecules directly form a layer on the charged nanospheres, and thus electrical double layers (EDL)[135] will be generated which prevent the further aggregation to some extent, as shown in Figure 3. In the case of non-polar liquids, no such formation of electrical double layers is possible, and hence the aggregation of the fragments takes place until the disappearance of the smaller fragments occurs. As a result, the average size of the Al NPs in the CCl_4 was ~30 nm (range of 10 nm–50 nm), while in $CHCl_3$ it was ~15 nm (range of 5 nm–35 nm). UV-Vis absorption spectra recorded for the both colloids also strengthened the

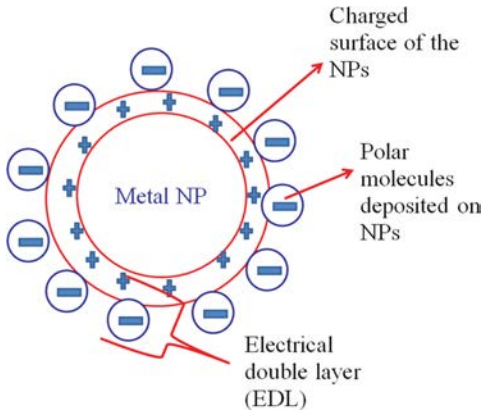

Figure 3. Electrical double layer (EDL) formed on the charged surface of the Al NPs to prevent further aggregation.

observation that NPs with lower average size in $CHCl_3$ compared to CCl_4 were formed through exhibition of the SPR peaks at 270 nm and 300 nm, respectively.[136] In addition to the fabrication of different-sized NPs, NSs of different morphologies were also observed as. A similar experiment has been carried out with ~2 ps laser pulses to distinguish the fs ablation with ps ablation, and the obtained results are presented in Figures 4 and 5. Morphology and crystallinity of the fabricated Al NPs were observed to depend on the liquid in which ablation is carried out. Depending on the position of the focus, micro structures and NSs were observed on the target as shown in Figure 6. Displacement of the focus in the liquid media is the one of the reasons to observe microstructures or NSs on the surface. Al NSs fabricated in the CCl_4 and $CHCl_3$ can be used for trace-level detection through recording the Raman spectra of the adsorbed analytes with an excitation wavelength in the UV spectral range.

3.2. Effect of Beam Waist and Multiple/Double/Single Line Ablation on the Nanomaterials

Rather than the individual effect of laser spot and the number of laser pulses per spot, a combined effect of the two was investigated for the Ag substrate immersed in double-distilled water at a wavelength of 800 nm.[137] The experiment was carried out with the experimental parameters with ~2 ps pulses. Periodic structures on the Ag substrate with separations of 5 μm, 25 μm, 50 μm, and 75 μm were fabricated. Typical energy used was ~150 μJ per pulse. The schematic of multiple/double/single line ablation carried out on the Ag substrate is documented in our earlier work.[137] Scanning speeds of the X–Y stages were 0.4 mm/sec and 0.5 mm/sec. The prepared Ag colloids are designated as NP-1, NP-2, NP-3 and NP-4, and the corresponding substrates as SS-1, SS-2, SS-3, and SS-4, for separations of 5 μm, 25 μm, 50 μm, and 75 μm, respectively. The theoretical beam waist (ω_0) estimated at the focus (in air) was ~20 μm. SS-1 was influenced by

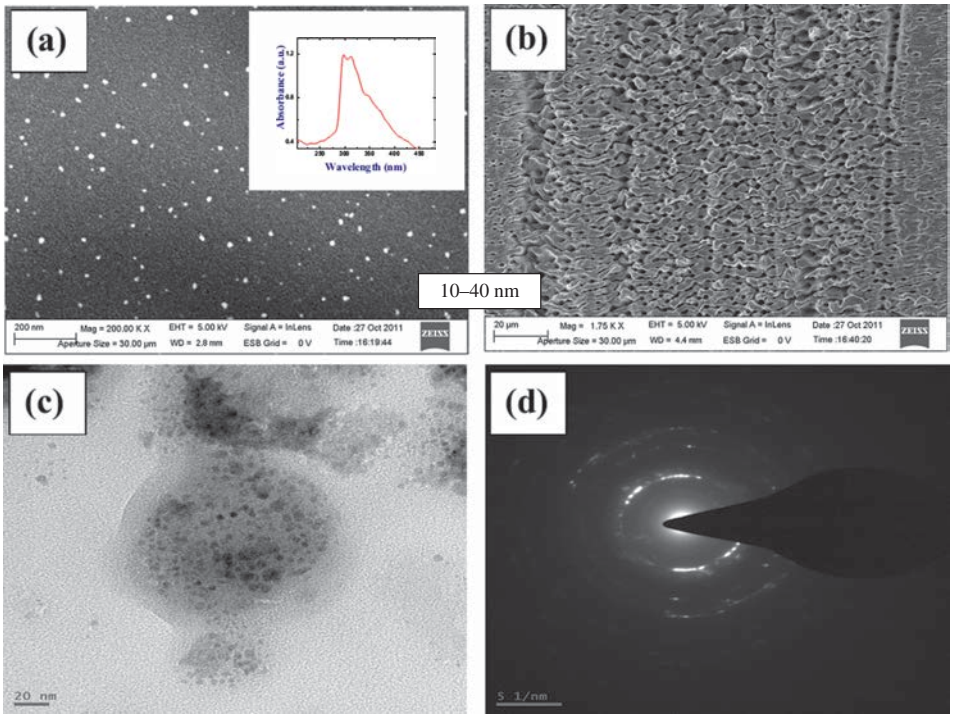

Figure 4. (a) FESEM images of the Al NPs in carbon tetrachloride and inset depict UV-Vis absorption spectra of CCl_4 colloidal solution was showing two peaks near 297 nm and 313 nm and a small hump near 350 nm. (b) Al substrate exposed to 2 ps laser beam. (c) TEM imaging of the Al NPs. (d) SAED pattern.

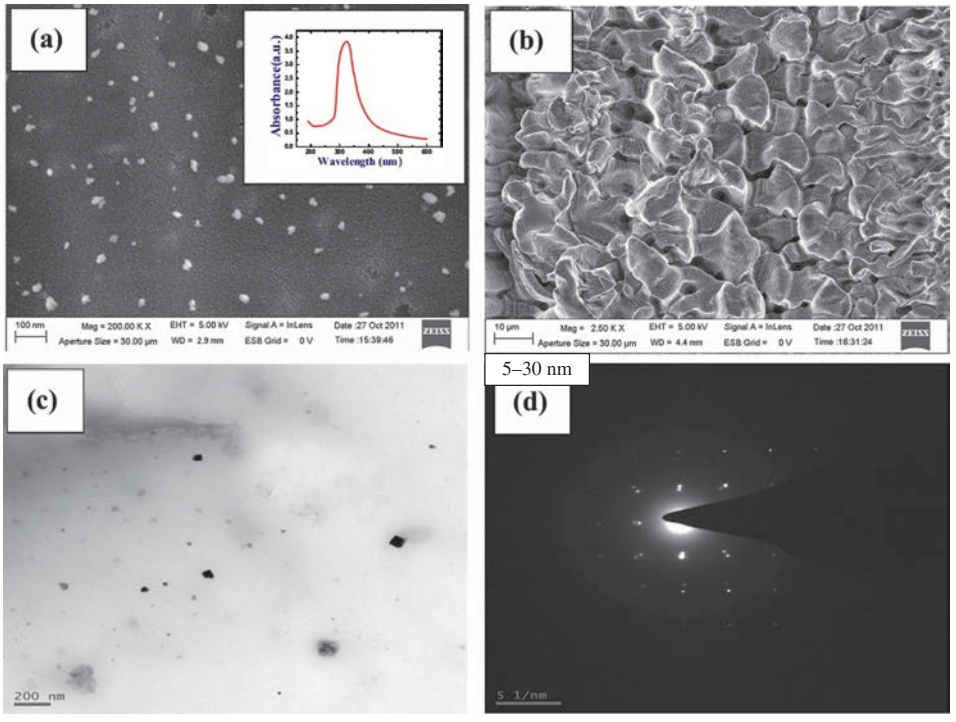

Figure 5. (a) FESEM images of the Al colloids in chloroform and inset depict UV-Vis absorption spectra of the chloroform colloidal solution was showing a peak near 323 nm. (b) Al substrate exposed to ~2 ps laser beam. (c) TEM imaging of the Al NPs. (d) SAED pattern of Al NPs.

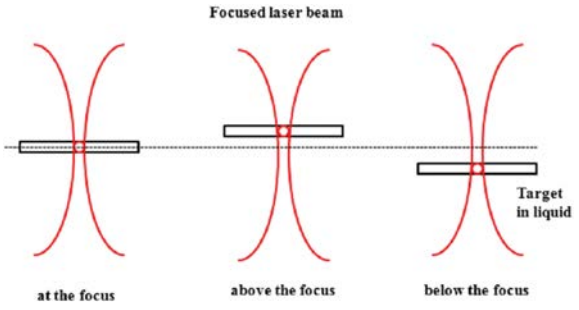

Figure 6. Focused laser beam onto the surface of the target immersed in liquid. Displacement of the focus results in various micro and NSs on the target surface.

multiple line ablation, whereas SS-2 was influenced by double line ablation, since the estimated beam waist on the Ag substrate was > 20 μm. Consequently, complete overwriting (ablation of the pre-ablated portion) was carried out for SS-1 and partial overwriting for SS-2. Apart from these, SS-3 and SS-4 were obtained through a single line ablation. Furthermore, Ag substrates for double line ablation were also fabricated at different fluences of 4 J/cm^2, 8 J/cm^2, 12 J/cm^2, 16 J/cm^2, and 20 J/cm^2.

Analysis of both the NPs and NSs revealed that double line ablation resulted in the fabrication of Ag substrates with dome-like structures, multiple line ablation revealed a better yield of NPs, and single line ablation was observed to give small-sized Ag NPs (7 nm). In our case the ablation of pre-ablated substrate occurs multiple times on SS-1, since the separation between the two line structures (5 μm) was less than the estimated spot size on substrate. Ablation for the first time creates initial roughness (micro-protrusions), and for the second time (on the first ablated portion) roughness offered will not be uniform, leading to inhomogeneous melting of tips and micro-protrusions; consequently, threshold fluence decreases, resulting in higher yield of NPs, and Nielsen et al.[131] demonstrated that the roughness provided by ablation for overwriting caused laser-induced surface plasmons and surface-scattered waves, which led to the coupling of laser energy to the modified surface in the next step of overwriting. Double line ablation of Ag substrate was ablated at different fluences and the fabricated Ag NPs are shown in Figure 7. It was observed that the yield of the NPs along with double line ablation was increased with fluence, as shown in Figure 8(a). UV-Vis absorption spectra of the Ag colloids showed the difference in the average

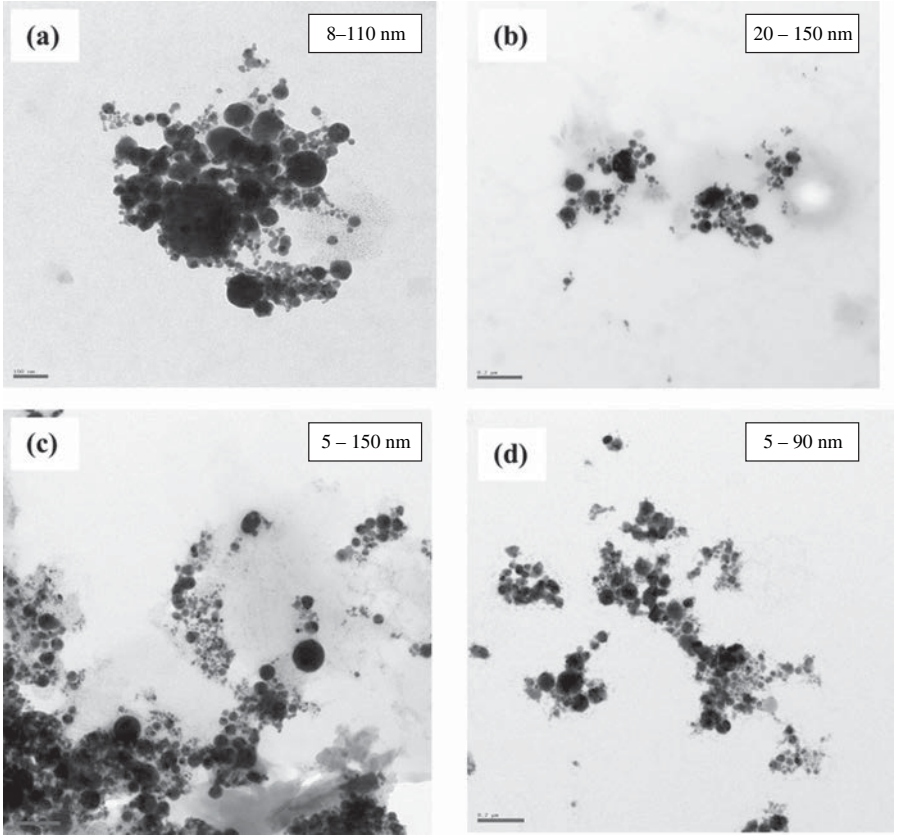

Figure 7. TEM imaging of Ag NPs prepared for (a) 4 J/cm^2 (b) 8 J/cm^2 (c) 12 J/cm^2 (d) 16 J/cm^2 in distilled water with $\sim$2 ps laser pulses.

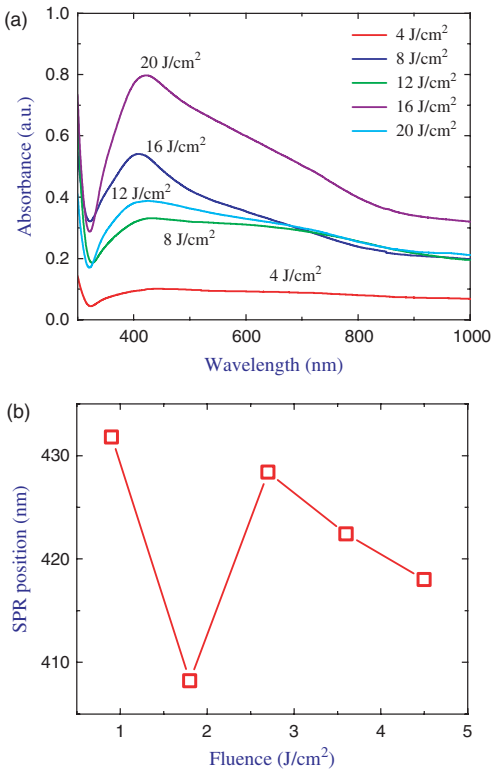

Figure 8. (a) UV-Vis spectra of the Ag NPs in water prepared for different laser fluences. (b) SPR shift of Ag colloids in water with respect to input fluence.

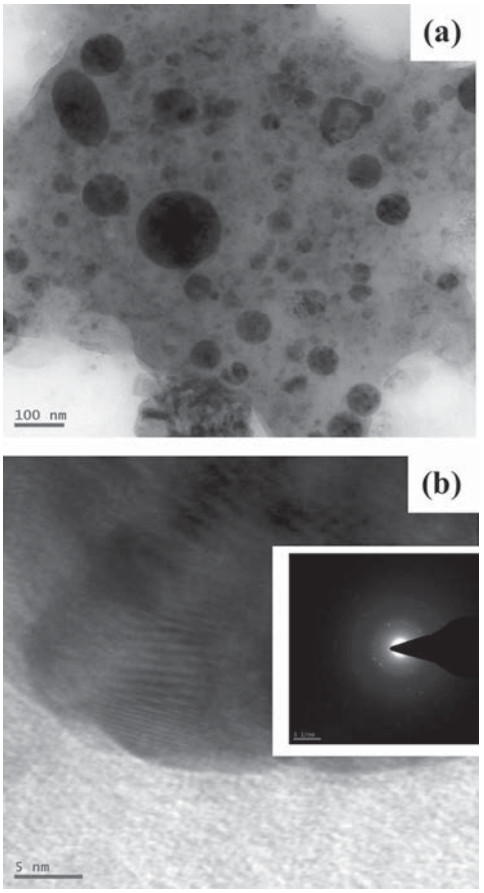

Figure 9. (a) TEM imaging of Cu NPs prepared with a fluence of 8 J/cm^2 in distilled water and ~2 ps laser pulses, and (b) HR-TEM image of Cu NPs and inset shows the SAED pattern of Cu NPs.

sizes and distribution, as shown in Figure 8(b). Ablation of the different targets submerged in various aqueous media through ultrafast laser pulses and their outcomes are listed in Table I.[138–152] In addition, the effect of liquid medium on the outcomes of the ablation in different liquid media was carried out and documented[153–155] to utilize the fabricated silver nanomaterials for different applications. In a similar fashion, Cu NPs were fabricated in double-distilled water with 2 ps laser pulses, as shown in Figure 9. Ag substrates corresponding to the ablation at different fluences in water as mentioned above are depicted in Figure 10, which revealed fabrication of pillar-like structures in the laser exposed portions.

LAL is utilized with both ns and fs pulses to produce many other nanomaterials such as Ge,[156–157] silicon,[158–159] GaAs,[160] antimony sulphide,[161] and zinc,[162] Mg/MgO,[163] Ti/TiO_2,[164, 165] and ceramic (Si_3N_4, SiC, AlN and Al_2O_3) NPs,[166, 167] to name a selected few. LAL generally supports gram-scale synthesis of metallic/semiconductor/ceramic NPs, and it is tough to fabricate higher yields greater than gram scale. Parallel processing with multiple beams is one of the possibilities to increase yields. Size distribution of the NPs is mostly affected by the post-ablation dynamics in the colloidal solution. Even the individual effect of laser parameters and solvent on the outcome of the ablation is explained to the date these parameters are interrelated. Unlike some of the chemical methods used for nanomaterials synthesis, ULAL at the moment, probably, provides modest control on the shapes of the nanostructures fabricated over a large area (a few inches).

4. APPLICATIONS

4.1. Surface Enhanced Raman Scattering of the Analytes Adsorbed on the Nanostructured Metallic Substrates

Raman scattering is a weak process with extremely small cross sections (~10^{-31}–10^{-26} cm^2/molecule) leading to a poor signal-to-noise ratio, since it originates from the second order perturbation term. Due to this reason, spontaneous Raman scattering fails to deliver decisive information of molecular fingerprints in the trace detection. Ambiguity in detection was eliminated by employing surface-enhanced Raman scattering [SERS].[168–176] SERS technique has recently caused a great deal of excitement, since it was found experimentally that the effective Raman cross sections of molecules on, for example,

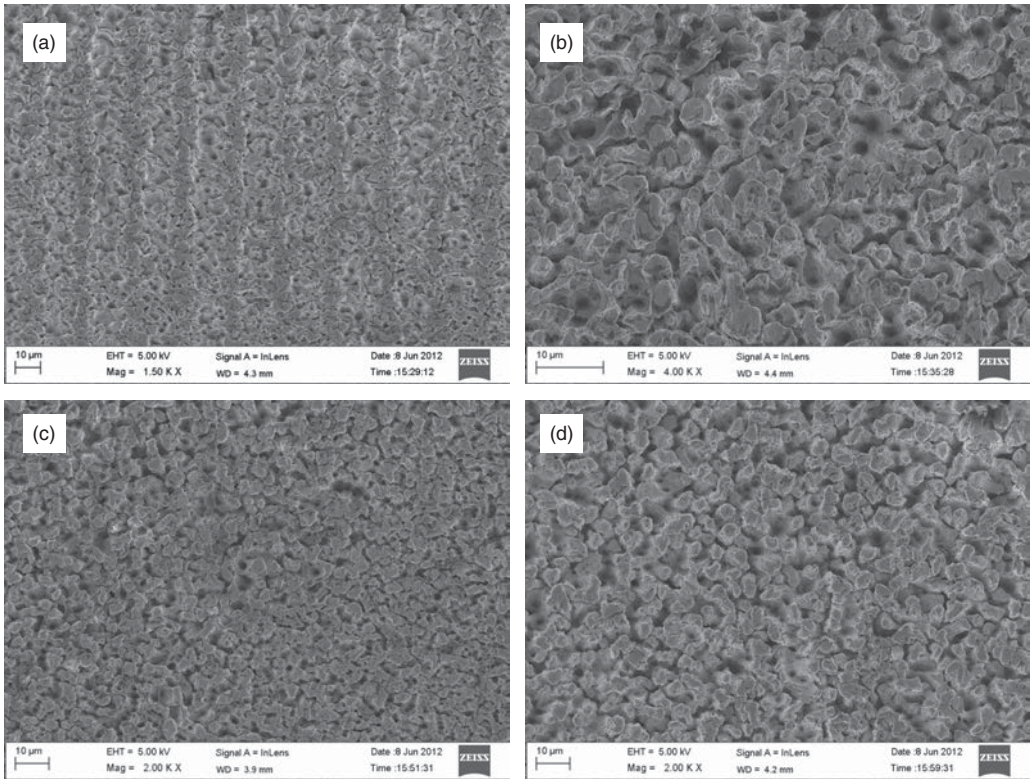

Figure 10. FESEM imaging of the laser ablated Ag substrates in water with ~2 ps laser pulses at fluence (a) 4 J/cm^2 (b) 8 J/cm^2 (c) 12 J/cm^2 (d) 16 J/cm^2.

a roughened silver (plasmonic metal) surface can be 10^5–10^7 times larger than those of the same molecules in solution by Fleischman way back in 1974.[168] He proposed that enhancement might occur from the increased surface area; i.e., number of molecules. In 1977 Jeanmaire and Van Duyne[169] explained the observed strong Raman signals of pyridine on the rough silver could be from the true enhancement of Raman-scattering efficiency itself. Albrecht and Creighton[170] also proposed similar arguments independent to the former two reports. After few years this effect was verified by observed Raman enhancements of different molecules adsorbed on the roughened plasmonic metal substrates consisting of NSs of dimensions of a few tens of nm.[171] Deployment of SERS spectroscopy allowed for the overcoming of sensitivity problems with giant Raman enhancements[172–176] of ~10^7–10^8. Single-molecule detection studies demonstrated that enhancements of order 10^{14}–10^{15} are also possible at the specific sites of the nanomaterials arrays, which were designated as hot spots.[177–179] The main objects that can be employed in SERS are the nanosized colloidal suspensions and nanostructured substrates of the plasmonic metals such as silver, gold, and copper, since these nanoentities can create a platform providing plasmon oscillations. Plasmons are the quantum of collective oscillations of conduction electrons (free electrons) in the surface of the nanomaterials. The peculiar characteristics of the plasmonic metals are ascribed to their complex dielectric function, with large negative quantities of real parts responsible for polarization of the material under the influence of the incident field and the positive imaginary part contributing to the optical absorption. ULAL is a suitable method to fabricate both NPs and NSs in single experiment, and has potential for utilizing both NPS and NSs as SERS active elements.

Most of the experiments performed for detection of organic molecules were carried out with the chemically synthesized plasmonic metal NPs and NSs.[180–183] Lack of reproducibility of the NPs with the same size and NSs with similar surface morphologies limited the usage of nanomaterials fabricated through pulsed LAL. Lee et al.[184] reported an enhancement factor of order 10^5 for benezenethiol (10 μM) molecules adsorbed on Ag (15 nm) and Au (18 nm) nanoparticle colloids, NSs fabricated by laser ablation in triple-distilled water with 7 ns laser pulses. Raman spectrum was recorded from the analytes adsorbed on Ag nanomaterials, Au nanomaterials with excitation wavelengths 514.5 nm and 632.8 nm, respectively. Lau et al.[51] fabricated Ag, Au, Ta and Ti NSs in water with 350 ps pulses and SERS activity of acridine molecules of the concentration 10 μM were investigated for different laser shot numbers of excitation wavelength 514 nm, and observed a better elevation of Raman

signatures at a higher number of laser shots. Many groups have demonstrated the utility of Au, Ag, and Cu nanomaterials for detection of various organic and explosive compounds.

Raman signal enhancements of the R6G and RDX ($C_3H_6N_6O_6$; 1,3,5-Trinitroperhydro-1,3,5-triazine) were investigated through the doubly ablated silver substrates. It was detected that the maximum enhancement of Raman signals were observed from the RDX molecules adsorbed on Ag substrates fabricated at the fluences of 12 J/cm^2 (532 nm excitation) and 16 J/cm^2 (785 nm excitation). Ag nanoparticle grains in the NSs could possibly have generated hot spots for the observed signal enhancements.[137] After appropriate cleaning, the same substrates were utilized to record Raman spectra of TNT molecules dissolved in acetonitrile, and we observed good signal elevation from the molecules adsorbed on these substrates and the data is shown in Figure 11. Observed Raman modes were assigned as C—H asymmetric stretching vibrations corresponding to 3009 cm^{-1} and C—H symmetric stretching vibration corresponding to 2947 cm^{-1}; both belonging to alky CH_3 group.

Other important peaks observed were 1622 cm^{-1} corresponds to 2,6 NO_2 asymmetric stretching, 1552 cm^{-1} corresponds to NO_2 asymmetric stretching, 1399 cm^{-1} corresponds to symmetric stretching corresponds, 924 cm^{-1} corresponds to C—H (ring) out of plane bend, and 324 cm^{-1} corresponds to 2, 4, 6 C—N in plane torsion. Enhancements of $\sim 10^2$ in the Raman intensities and enhancement factors of $\sim 10^3$–10^4 were observed for some of the modes investigated. We are in the process of extending these studies with bi-metallic nanostructured targets prepared using ULAL.

The majority of the reported experiments are a combination of laser ablation and chemical process; i.e., laser ablation of the metallic targets in solvents like ($AgNO_3$, $HAuCl_4$ ...), which fabricated the NSs with metal ions deposition from the solvent used. Siskova et al.[185] investigated the effect of various ions on the product of ablation and revealed that ablation of metal targets in NaCl and HCl produce more stable NPs than ablation in NaOH, pure water, THS and $AgNO_3$. Similarly, two-step fabrication of SERS active substrates through the coating of the ultrafast laser ablated semiconductors (Si) surfaces with gold or silver are also under tremendous development, since their outcomes end up with a beautiful ripple pattern. Buividas et al.[186] fabricated ripple structures on sapphire substrate with 150 fs laser pulses, and later gold or silver coating on the roughened surface was carried out, and recorded enhanced Raman signal of thiophenol from the silver/gold coating. Exclusive data of the latest SERS studies[187–202] of the plasmonic metal targets in liquid media is listed in Table II.

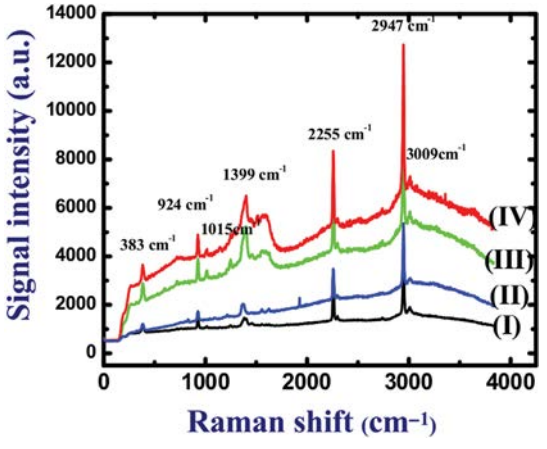

Figure 11. Micro-Raman spectra of adsorbed TNT molecules (excitation at 532 nm) dissolved in acetonitrile and placed on nanostructured Ag. The maximum enhancement of Raman signal was observed at pulse energy 150 μJ (fluence of 12 J/cm^2). The time of integration was 5 s. 4 J/cm^2–(I), 8 J/cm^2–(II), 12 J/cm^2–(III) and 16 J/cm^2–(IV).

4.2. Nonlinear Optical Studies of the Colloidal NPs

The development of photonic devices to process information with large speeds (using all-optical techniques) has been the motivation for materials scientists to synthesize and investigate novel nonlinear optical (NLO) materials. There are large numbers of novel materials fabricated for NLO applications with fs or ps time response.[203] The attention on new NLO materials has been confined mainly to the progress of optical limiters for sensor protection,[204] mode-locking elements,[205] in optical switching,[206] etc. NLO materials are also interesting in the development of technologies in the fabrication of waveguides[207, 208] with intensity-dependent refractive indices. A variety of large NLO properties has been established by metal NPs in different solvents, which were fabricated via different methods.[209–222] Metal NPs are promising compared to other NPs due the advantages from the viewpoint of surface plasmon resonance (SPR).[223, 224] The unique NLO properties of metal NPs can be attributed to their SPR bands. Noble metal NPs have been proved to be attractive for their large NLO coefficients and ultrafast response times[225, 226] due to the enhancement of local electric fields in the vicinity of the SPR band. It is also important to manufacture potential NLO materials possessing strong NLO coefficients in the near IR region, which are capable for applications in the area of telecommunications.

Herein, some results from NLO studies of metal NPs synthesized via ULAL at 800 nm (Ti: Sapphire, $\sim$2 ps pulses, $\sim$40 fs pulses) utilizing Z-scan technique are presented. Ps pulses were generated by Ti: sapphire amplifier (Coherent, Legend) operating at a repetition rate of 1 kHz. The amplifiers were seeded with $\sim$15 fs pulses from the oscillator (Coherent, Micra). The input beam was spatially filtered to obtain a pure Gaussian profile in the far field. Z-scan studies[227–230] were performed by focusing the 3 mm diameter input beam using a 200 mm focal length convex lens into the sample in the ps domain. The experiment was

Table II. Summary of reports on NPs and NSs generated using ULAL and utilizing them for SERS studies.

Material	Medium	Source	Size (nm)	Analyte	EF#	Ref.
Ag foil	Water	1064 nm 10 Hz 20 ns	40 12.5	5,10,15,20-tetrakis (1-methyl-4-pyridyl) porphyrin (10^{-7} M)		[187]
Ag foil	Water 2,2′, bipyridine phtalazine	1064 nm 1 Hz 40 ps		2,2′, bipyridine phtalazine (10^{-6} M)		[188]
Ag foil	Water, 2,2′, bipyridine, phtalazine, 2,3,5,6-tetrakis (2′-pyridyl) pyrazine	1064 nm 1 Hz 40 ps		2,2′, bipyridine, phtalazine, 2,3,5,6-tetrakis (2′-pyridyl) pyrazine (10^{-5} M)		[189]
Ag and Au (NPs and NSs)	Triple-distilled water	1064 nm 1 Hz 6 ns	15 18	Benzenethiol (10^{-5} M)	10^5	[190]
Ag	Water	1064 nm 10 Hz 20 ns		5,10,15,20-tetrakis-(1-methyl-4-pyridyl) porphyrin [10^{-5} M]		[191]
Ag	Water	1064 nm 10 Hz 6 ns	30	5,10,15,20-tetrakis (1-methyl-4-pyridyl) porphyrin [10^{-7} M]		[192]
Ag	Water	1064 nm 6–9 Hz		*p*-hydroxy benzoic acid		[193]
Gold	Water	1064 nm 10 Hz 3–6 ns	30–100	5,10,15,20-tetrakis (1-methyl-4-pyridyl) porphyrin (10^{-7} M)		[194]
Ag and Au (NPs and NSs)	Water	1064 nm 10 Hz 10 ns	3–30	Adenine (10^{-8} M)	10^9	[195]
Ag	Water, Hcl NaCl, NaOH $AgNO_3$	1064 nm 10 Hz 20 ns		2,2′ bipyridine (10^{-6} M)		[185]
Ag	Water 2,2′, bipyridine	1064 nm 532 nm	10–15	2,2′, bipyridine (10^{-5} M), 5,10,15,20-tetrakis (1-methyl-4-pyridiniumyl)-21H, 23H porphine (10^{-7} M)		[196]
Cu	Acetone, water 1,10-phenanthroline, 4,4′ bipyridine	1064 nm 10 Hz 10 ns	3–9 10–30	1,10-phenanthroline, 4,4′ bipyridine		[197]
Ag Au Cu	Water	1064 10 Hz 38 ps		4-mercaptopyridine (10^{-3} M)		[198]
Ag	Methanol	532 nm 30 Hz 6 ns	35	R6G (10^{-7} M) (10^{-15} M)	10^6 10^{12}	[199]
Ag [AgCl cubes]	NaCl solution [0.005 M]	248 nm, 10 Hz, 30 ns	100–200	R6G (10^{-11}–10^{-5} M)		[200]
Au	Water, acetone	1064 nm, 10 Hz, 25 ps; 532 nm, 10 Hz, 20 ps	10 2–3	1,10 phenanthroline		[201]
Cu Cu/Ag bi-functional NPs	$AgNO_3$	1064 nm, 10 Hz, 25 ps	3 ± 1.6	1,10 phenanthroline		[202]

Note: # EF: Enhancement factor.

performed with the samples placed in 1 mm glass/quartz cuvette, which was positioned on a high resolution translation stage and the detector (Si photodiode, SM1PD2A, Thorlabs) output was connected to a lock-in amplifier. Both the stage and lock-in amplifier were controlled by a computer program. The samples were translated insteps of 1 mm along the *Z*-axis direction when scanning through the focal region. The nonlinear absorption studies were performed by an open aperture (OA) Z-scan method with different peak intensities to completely understand the intensity-dependent nonlinear absorption. To determine the nonlinear refraction of metal NPs we used closed aperture

(CA) Z-scan technique. These CA studies were performed at lower peak intensities where the contribution from the higher order nonlinear effects is negligible (the value of $\Delta\phi$ stimated in all the cases was $< \pi$).

The NLO mechanisms mainly observed in the case of metal NPs[231–234] are saturable absorption (SA), switching case [SA in reverse saturable absorption (RSA) or RSA in SA] and simultaneous two/three photon absorption (2PA or 3PA). Experimentally observed SA, switching and simultaneous 2PA cases of metal NPs can be attributed to the intra-band (or) inter-band transitions. The occurrence of SA[233] is possible in two cases with excitation at 800 nm (1.55 eV) (a) intra-band electronic excitations within the conduction band occurring at lower peak intensities in the vicinity of SPR,[234] and (b) inter-band electronic excitations taking place from *d*-band to *s*- (or) *p*-band. Further pumping leads to excitation into higher excited states in the conduction band, since the free-carrier absorption cross-section will be significant at higher peak intensities, and this is reflected in the switching from SA to RSA. Further pumping (highest peak intensities) resulted the observation of 2PA/3PA since the electrons, through intra-band transitions, can be excited from the ground state of conduction band to higher-lying excited states of conduction band (or) *d*-band to higher-lying excited states of conduction band (inter-band transitions) via simultaneous absorption of two/three photons, depending on the photon energy and the band gaps. To fit the experimental data of switching from SA to reverse-saturable absorption (RSA), we combined saturable absorption coefficient and two photon absorption (TPA, β) coefficients yielding the total absorption coefficient[235, 236] as

$$\alpha(I) = \alpha_0 \frac{1}{1 + I/I_S} + \beta I \tag{1}$$

$$I = \frac{I_{00}}{1 + (z/z_0)^2} \tag{2}$$

where the first term describes the negative nonlinear absorption and the second term describes positive nonlinear absorption, such as reverse saturable absorption and/or two-photon absorption, α_0 is the linear absorption coefficient. I_{00} and I_S are laser peak intensity and saturation intensity, respectively. β is the positive nonlinear absorption coefficient.

In the presence of saturable absorption[237–239] only the first term of Eq. (1) needs to be considered.

$$\alpha(I) = \alpha_0 \frac{1}{1 + I/I_S} \tag{3}$$

Using Eqs. (1) and (2), I_s and β can be obtained from the open aperture Z-scan data by fitting it to the following equation

$$\frac{dI}{dz'} = -\alpha(I)I \tag{4}$$

where z' corresponds to sample length. If the excitation intensity I is lesser than I_s, we can consider SA as a third-order process, and in such cases $-(\alpha_0/I_S)$ is the equivalent of nonlinear absorption coefficient β (negative nonlinear absorption), to a good approximation. $\mathrm{Im}[\chi^{(3)}]$ can be evaluated from the coefficient β.[239] Assuming a spatial and temporal Gaussian profile for laser pulses, and utilizing the open aperture Z-scan theory for two photon absorption (2PA) given by Sheik-Bahae et al.[240] the equation for 2PA open aperture (OA) normalized transmittance given by[240–242]

$$T_{OA}(2PA) = \frac{1}{\pi^{1/2} q_0(z,0)} \times \int_{-\infty}^{\infty} \ln[1 + q_0(z,0)\exp(\tau^2)]\, d\tau \tag{5}$$

For $|q_0| < 1$ and ignoring the higher-order terms, we obtain,

$$T_{OA}(2PA) = 1 - \beta I_{00} L_{\mathrm{eff}}/(1 + (z/z_0)^2)2^{3/2} \tag{6}$$

Three-photon absorption (3PA) equation is

$$T_{OA}(3PA) = \frac{1}{\pi^{1/2} p_0} \int_{-\infty}^{\infty} \ln\{[1 + p_0^2 \exp(-2\tau^2)]^{1/2} + p_0 \exp(-\tau^2)\}\, d\tau \tag{7}$$

For $|p_0| < 1$, and ignoring the higher-order terms, we obtain,

$$T_{OA}(3PA) = 1 - 2\gamma I_{00}^2 L'_{\mathrm{eff}}/(1 + (z/z_0)^2)3^{3/2} \tag{8}$$

where,

$$q_0(z,0) = \frac{\beta I_{00} L_{\mathrm{eff}}}{1 + (z/z_0)^2}, \quad p_0(z,0) = \frac{2\gamma I_{00}^2 L'_{\mathrm{eff}}}{1 + (z/z_0)^2}$$

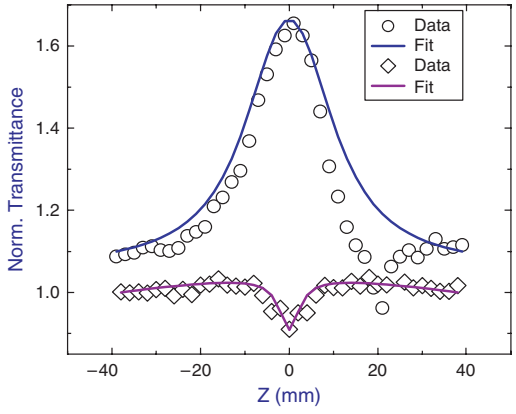

Figure 12. Open aperture ps Z-Scan curves obtained for Al NPs in CCl_4 (open circles) and Al NPs in $CHCl_3$ (open squares) $I_{00} = 55$ GW/cm.^{2} Open symbols are experimental data points while solid curves are theoretical fits. The top curve is shifted for clarity.

Table III. Details of reports on synthesis of NPs through ULAL of metals and their NLO coefficients.

Sample	Laser ablation parameters	NLO study parameters (wavelength and pulse width)	β (or) α_2 (cm/GW) [I_s (GW/cm^2]	n_2 (cm^2/W)	$\lvert\chi^{(3)}\rvert$ (e.s.u.)	Ref.
Ag NPs	7 ps, 515 nm	Q-switched Nd:YAG laser	β/n'' (cm^2/J) $= 14.9 \times 10^{-3}$			[243]
Au NPs Ag + Au NPs	(33.3 kHz)	3 ns, 532 nm (3 Hz)	8.1×10^{-3} 5.4×10^{-3}			
(methyl 2-methylprop-2-enoate liquid)	All samples @ 1064 nm	13.5×10^{-3}				[243]
Au (gold) and Ag (silver) NPs in water	Q-switched Nd:YAG laser 532 nm, 355 nm and 266 nm (7 ns, 10 Hz)	532 nm and 7 ns (10 Hz)	47.37 8.17		7.5×10^{-11} 1.8×10^{-11} (imaginary part)	[243]
Ag NPs (ethylene glycol, water, or ethanol)	Q-switched Nd:YAG laser 532 nm, (9 ns, 10 Hz)	(a) Ti:sapphire laser, 1.2 ps, 397.5 nm (10 Hz) (b) 800 fs, 795 nm (c) Nd:YAG laser 397.5 nm, 8 ns, (1 Hz)	-1.5 8.0 3.0	3×10^{-13}	2×10^{-12} 3×10^{-8} (imaginary part)	[244]
Ag NPs (distilled water)	Copper vapor laser 510.6-nm, 20 ns (15 kHz)	LTI-404 Nd :YAG laser, 25 ns, 532 nm (10 Hz)	-10.4 -3.7			[245]
Ag NPs Au NPs Ag + Au NPs	Q-switched Nd:YAG laser 532 nm, (240 ns, 210 Hz)	Q-switched Nd:YAG laser 532 nm, 10 ns, (300 Hz)	25.7 27 26.5	-2.27×10^{-13} -3.78×10^{-13} -8.13×10^{-13}	5.64×10^{-5} 3.23×10^{-5}	[246]
Ni (nickel) in ethanol	Q-switched Nd:YAG laser 1064 nm, (240 ns, 2 kHz)	CW He–Ne laser beam, 632.8 nm	79×10^4 116×10^4 150×10^4	-3.04×10^{-7} -2.12×10^{-7} -1.75×10^{-7}		[247]
	Q-switched Nd:YAG laser 532 nm, (10 ns, 200 Hz)	7×10^4	-8×10^{-11}			[247]
Al NPs in CCl_4 and chloroform	Ti:sapphire laser, 40 fs and 800 nm (1 kHz)	Ti:sapphire laser, 2 ps and 800 nm (1 kHz) Al NPs-CCl_4 ($I_{00} = 55^*$, 96, 130 and 190 GW/cm^2)	0 [2]* 0.19 [6.5] 0.33 [5] 2		0.64×10^{-11} 1.1×10^{-11} 6.7×10^{-11} (im. part)	Present work [136]
		Al NPs-$CHCl_3$	0.023[0.032]*			Present work
		($I_{00} = 55^*$, 69, 110 and 140 GW/cm^2)	0.049[6] 0.05 0.063		1.6×10^{-12} 1.7×10^{-12} 2.1×10^{-12}	[136]
Ag NPs in water	Ti:Sapphire laser, 2 ps and 800 nm (1 kHz).	Ti:Sapphire laser, 2 ps and 800 nm (1 kHz) NP-1 ($I_{00} = 83$, 138 GW/cm^2)	2×10^{-3} [0.065] 4.5×10^{-3}	3.4×10^{-16}	2.29×10^{-14}	[137]
		NP-2	6.2×10^{-3} 1.78×10^{-2}	4×10^{-15}	2.69×10^{-13}	[137]
		Ag NPs in water (single ablation) $I_{00} = 170^*$ GW/cm^2	$\gamma* = 1.5 \times 10^{-21}$ cm^3/W^2			Present work
Cu NPs	Ti: sapphire laser, 2 ps and 800 nm (1 kHz).	Ti: sapphire laser, 2 ps and 800 nm (1 kHz) Cu NPs in $CHCl_3$	$\gamma = 1.3 \times 10^{-20}$ cm^3/W^2			Present work
		Cu NPs in DCM	$\gamma = 7.9 \times 10^{-22}$ cm^3/W^2			Present work
ZnO NPs in water	Ti: sapphire laser, 2 ps, 800 nm (1 kHz)	Ti: sapphire, 2ps, 800 nm (1 kHz)	$\gamma = 2.5 \times 10^{-22}$ cm^3/W^2	1.46×10^{-12}		Present work
		ZnO -1 ZnO-2	$\gamma = 5.7 \times 10^{-22}$ cm^3/W^2	3.4×10^{-12}		

Note: *denotes the NLO coefficient value obtained at corresponding peak intensity mentioned in the previous column.

I_{00} is the peak intensity, z is the sample position, $z_0 = \pi\omega_0^2/\lambda$ is the Rayleigh range: ω_0 is the beam waist at the focal point ($z = 0$), λ is the laser wavelength; effective path length in the sample of length L for 2PA, 3PA is given as

$$L_{\text{eff}} = \frac{1 - e^{-\alpha_0 L}}{\alpha}, \quad L'_{\text{eff}} = \frac{1 - e^{-2\alpha_0 L}}{2\alpha_0}$$

4.2.1. Aluminum (Al)

Aluminum (Al) samples were prepared in liquid media via fs laser single line ablation by our group. The detailed description of preparation and characterization has been reported in one of our earlier articles.[136] Figure 12 illustrates the normalized transmittance of Al NPs fabricated in CCl_4 and in chloroform measured using open aperture Z-scan technique at a peak intensity of 55 GW/cm^2 (lower intensity). The transmission of the Al NPs in CCl_4 (open circles) was increased due to saturable absorption (SA) as they approached close to the focal point. In the case of Al NPs in $CHCl_3$ (open squares), the behavior demonstrated was switching from SA to reverse saturable absorption (RSA). The theoretical fitting was completed with the equations listed above. After fitting the experimental data we obtained saturation intensity $I_S = 2$ GW/cm^2 and $\beta = 0$ ($I_{00} > I_S$) for Al NPs in CCl_4 and $I_S = 3.2 \times 10^7$ W/cm^2 and $\beta = 2.3 \times 10^{-11}$ cm/W for Al NPs in $CHCl_3$ at a peak intensity of 55 GW/cm.^{2} Moreover, we reported about the same samples at higher peak intensities earlier.[136] The open aperture data of Al NPs in CCl_4 recorded at the same wavelength of 800 nm with three different peak intensities of 96 GW/cm,^{2} 130 GW/cm^2 and 190 GW/cm.^{2} The obtained behavior was SA and RSA in SA at lower- and medium-peak intensities, and at higher intensities behavior was modified to pure reverse saturable absorption (RSA) with strong two-photon absorption. For the case of Al NPs in $CHCl_3$, the open aperture data demonstrated the behavior was switching from SA to RSA at lower intensity (69 GW/cm^2), and it flipped to pure RSA with higher coefficients at higher intensities (110, 140 GW/cm^2). The reported magnitudes of coefficients are summarized in Table III.

4.2.2. Silver (Ag)

Ag colloidal NPs in water were recently prepared through ps laser double multiple line ablation by our group. The complete details of the prepared Ag NPs are mentioned in an earlier article.[137] The NLO study was performed on the colloids by Z-scan technique with 2 ps pulses at 800 nm. Figure 13 depicts the open aperture data Ag colloids in water via single line ablation [50 μm spacing between the lines] at a peak intensity of 170 GW/cm,^{2} and the data demonstrating the nonlinear absorption was three-photon absorption (3PA) with a coefficient $\gamma = 1.5 \times 10^{-21}$ cm^3/W,^{2} which could be due mainly to inter-band and/or intra-band transitions.

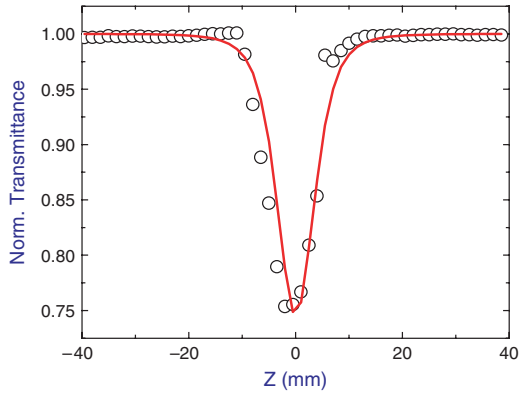

Figure 13. Open aperture ps Z-Scan curves obtained for colloidal Ag NPs in water fabricated via ps laser single ablation at a peak intensity of $I_{00} = 170$ GW/cm.^{2} Open symbols are experimental data points while solid curve is the theoretical fit.

Moreover, we reported open and closed aperture data of Ag colloids [NP-1, NP-2] prepared by ps laser multiple and double line ablation.[137] Open aperture Z-scan was carried out at peak intensities of 83 GW/cm^2 and 138 GW/cm,^{2} while the closed aperture data was recorded at 28 GW/cm.^{2} Open aperture data of NP-1 presented demonstrated switching behavior [from saturable absorption (SA) to reverse saturable absorption (RSA)], with a saturation intensity 6.5×10^7 W/cm^2 (and $\beta = 2 \times 10^{-12}$ cm/W) at lower-peak intensity (83 GW/cm^2). RSA with a strong two-photon absorption ($\beta = 4.5 \times 10^{-12}$ cm/W) was observed at higher-peak intensities (138 GW/cm^2). Observed switching behavior (from SA to RSA) and pure RSA of the Ag NPs were attributed to the intra-band transitions. The closed aperture data was fitted to extract the nonlinear refractive index (n_2). NP-1 exhibited positive nonlinearity and the measured n_2 was 3.4×10^{-16} cm^2/W. The open aperture data of NP-2 [linear transmittance (LT) $\sim$92%] indicating pure RSA for both lower ($\beta = 6.2 \times 10^{-12}$ cm/W) and higher ($\beta = 1.78 \times 10^{-11}$ cm/W) peak intensities. The retrieved coefficient n_2 for NP-2 from closed aperture data was 4×10^{-15} cm^2/W. The NLO coefficients of pure water from closed and open aperture data were also estimated. The n_2 value of the solvent was higher than the n_2 of NP-2, indicating that the sign of n_2 of NP-2 was negative. The measured $\chi^{(3)}$ (third-order NLO susceptibility) values for NP-1 and NP-2 were 2.29×10^{-14} e.s.u. and 2.69×10^{-13} e.s.u., respectively.

4.2.3. Copper (Cu)

NLO properties of copper (Cu) NPs in two different organic liquids (chloroform and dichloromethane) were investigated with $\sim$2 ps pulses at 800 nm wavelength at higher-peak intensity of 140 GW/cm.^{2} These Cu NPs were fabricated via ps single line ablation. All the other NLO data of Cu NPs in different solvents at other peak intensities (80 GW/cm^2 and 125 GW/cm^2) have been

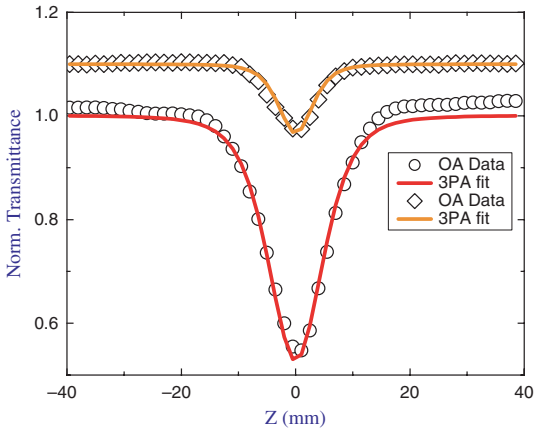

Figure 14. Open aperture Z-Scan curves obtained for colloidal Cu NPs in DCM (open squares) and chloroform (open circles) at a peak intensity of $I_{00} = 140$ GW/cm.^{2} Open symbols are experimental data points while solid curves are theoretical fits. The top curve is shifted for clarity.

reported elsewhere. The open aperture data of Cu NPs in chloroform and dichloromethane (DCM) have been illustrated in Figure 14. The observed nonlinear absorption was reverse saturable absorption (RSA) in both cases, and can be assigned to an effective three-photon absorption (3PA; γ) with coefficients of 1.3×10^{-20} cm^3/W^2 and 7.9×10^{-22} cm^3/W.^{2} Closed aperture data of Cu NPs exhibited both positive and negative optical nonlinearities, depending on the solvent used.

4.2.4. Zinc Oxide (ZnO)

ZnO NPs in water were fabricated by ps laser single line ablation at two different pulse energies 150 μJ (ZnO-1) and 200 μJ (ZnO-2). NLO properties of ZnO NPs were investigated at a wavelength of 800 nm. Figure 15 illustrates the SEM images [(a), (c)] and EDAX pictures [(b), (d)] of the ZnO NPs in water fabricated using 150 μJ and 200 μJ, respectively. Figure 16 depicts the UV-visible absorption spectra of the ZnO colloids fabricated in water using two different input energies of 150 μJ and 200 μJ. Figure 17 depicts (a) open aperture data of ZnO-1 (top) and ZnO-2 (bottom) with linear transmittance obtained at a peak intensity of 90 GW/cm^2 and (b) closed aperture data (right part) at a peak intensity of 70 GW/cm.^{2} The profile of open aperture Z-scan curves obtained was reverse saturable absorption (RSA) in both cases, and can be assigned to simultaneous/two-step three-photon absorption (3PA).

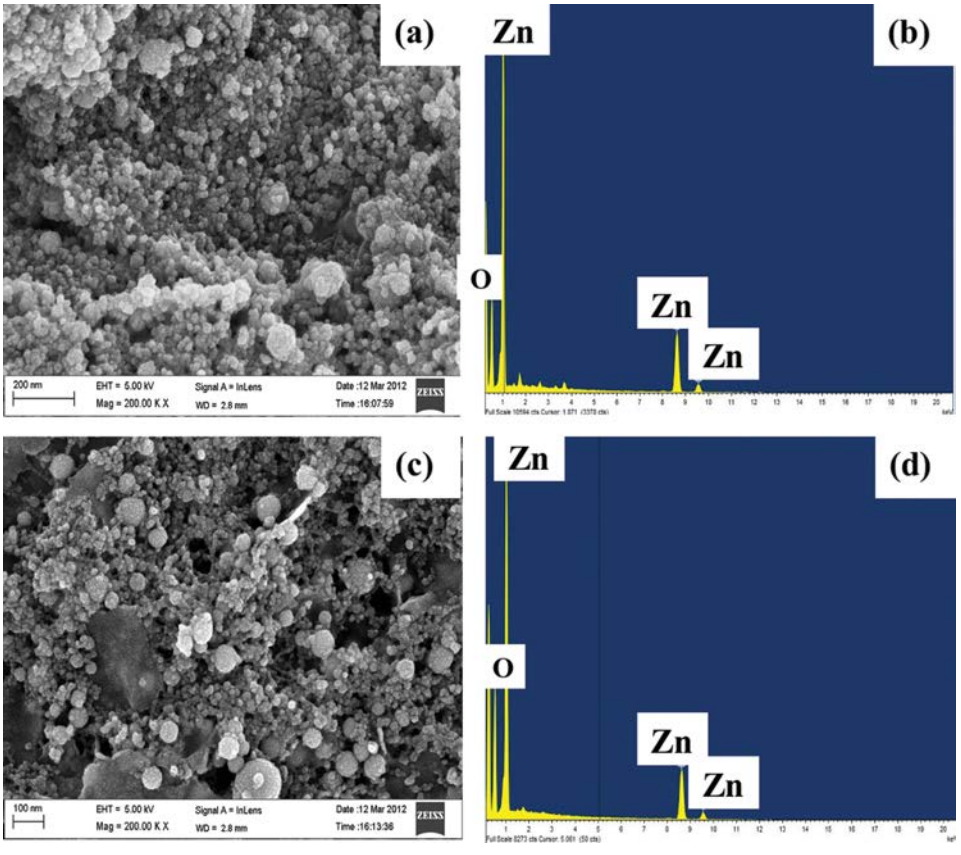

Figure 15. SEM imaging of colloidal ZnO NPs in water fabricated at two different energies (a) ZnO-1 (150 μJ) and (c) ZnO-2 (200 μJ), (b) and (d) are their respective EDAX pictures, confirming the nature of NPs.

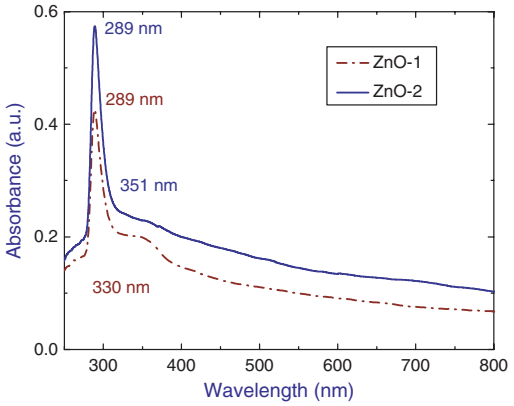

Figure 16. UV-Vis absorption spectra recorded for colloidal ZnO NPs in water fabricated at two different energies 150 μJ (ZnO-1, dashed-dotted curve) and 200 μJ (ZnO-2, solid curve).

The theoretical fits provided coefficients of an effective 3PA coefficient $\gamma = 2.5 \times 10^{-22}$ cm^3/W^2 for ZnO-1 and 5.7×10^{-22} cm^3/W^2 for ZnO-2, which can be attributed to the inter-band or intra-band transitions. Solid curves in Figure 17 are the theoretical fits obtained using the above-mentioned standard equations. Closed aperture Z-scan data for both samples revealed the positive nonlinearity with a high nonlinear refractive index 1.46×10^{-12} cm^2/W and 3.4×10^{-12} cm^2/W, respectively. The data was fitted[212–215] using standard equations to extract the nonlinear refractive index (n_2). Moreover, solvent (water) also exhibited nonlinearity, the magnitude of which was very small ($n_2 = 1.9 \times 10^{-15}$ cm^2/W) compared with ZnO NPs. Not many reports are available in literature on the NLO properties of metal NPs fabricated by ultrafast laser ablation in liquids.

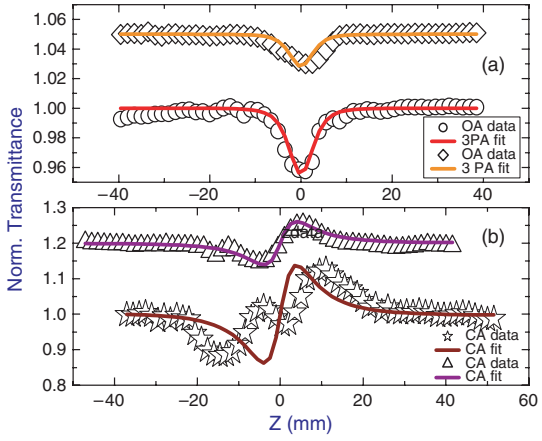

Figure 17. Z-Scan curves obtained for colloidal ZnO NPs in water fabricated with two different energies. (a) Open aperture data of ZnO-1 (open squares) and ZnO-2 (open circles). (b) Closed aperture data ZnO-1 (Open triangles) and ZnO-2 (open stars) at a peak intensity of $I_{00} = 90$ GW/cm.^{2} Open symbols are experimental data points while solid lines are theoretical fits.

The magnitudes obtained in our case are compared with reported coefficients of some of the synthesized NPs by ps and ns laser ablation.[243–247] One of the benefits of these NPs is that they can be used as such, or they can be incorporated into suitable polymer thin films; passive/active glasses with different functionalities and compositions to further improve their device capabilities.

4.3. Antibacterial Activities of Colloidal NPs

Dimensions and surface charge of metallic NPs such as copper/copper oxide (Cu/CuO), silver (Ag) and Al or Al_2O_3, etc have relevance to biological systems leading to antibacterial applications.[248, 249] Recent reports have demonstrated that Cu, and its oxidized, and Ag NPs have significant promise as antibacterial agents. In our case we have utilized the Ag NPs produced in acetonitrile to investigate the antibacterial activity of *E. coli* in the following methods.

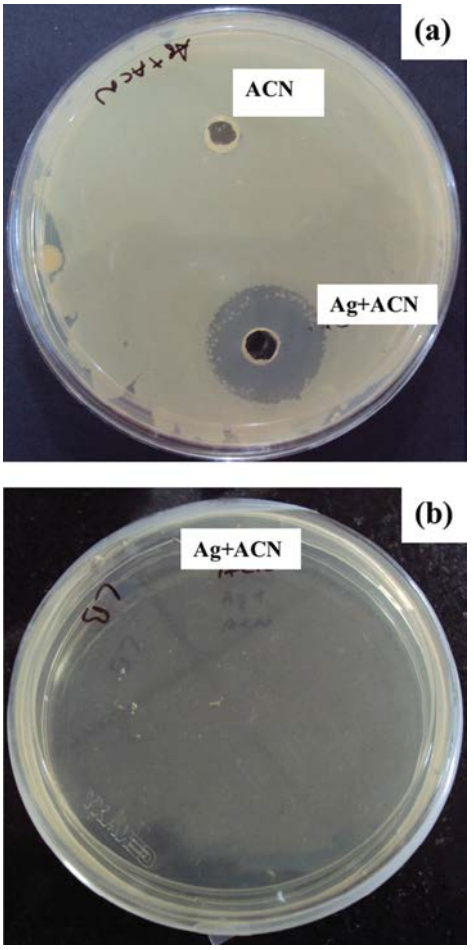

Figure 18. (a) E. coli zone of inhibition with Ag NPs in ACN in agar well diffusion method. (b) Agar plate of captured E. coli with Ag NPs in ACN in viability assay method.

4.3.1. Agar Well Diffusion and Viability Assay Methods

Investigation of antibacterial activity of Ag against E. coli gram negative bacteria by agar well diffusion and viability assay methods were performed. The bacterial suspension was applied uniformly on the surface of Muller-Hinton agar plates, and after 200 μl of Ag NPs was applied, their respective solvents have been filled in two agar wells. The plates were incubated at 37 °C for 24 h, and then the diameter of zone of inhibition was measured. In viability assay method *E. coli* culture was grown overnight in a LB. Aliquots of 100 μl of the culture were subcultured in fresh LB media (2 ml), and treated with Ag NPs and pure solvents; only inoculums without NPs served as negative control. Cultures were incubated for 3 hrs. 100 μl from each test was taken out for plating it on LB agar plates, incubated at 37 °C for overnight. Bacterial growth was investigated and colonies counted.[250] Figure 18 (c) clearly demonstrates the inhibition zones of E. coli provided by the silver NPs.

5. FUTURE PROSPECTS/DEVELOPMENTS

ULAL technique has the potential for creating unique NPs and NSs of a variety of materials. However, there are certain issues that need attention before it can be one of the most common techniques acceptable by physicists, chemists, and material scientists.[251–256]

1. ULAL technique needs to be customized in such a way to achieve a complete size, shape,[257] and distribution control of the NPs/NSs, with the intention of utilizing them according to the requirements in different fields.
2. Large-scale reproducibility should be improved in all ULAL studies through quantification of laser parameters and properties of the surrounding liquid media. Accordingly, a database should be prepared based on the already available and new literature.
3. An extensive theoretical work needs to be taken up to explain the dynamics underlying the fabrication of nanomaterials (NPs and NSs) in different temporal scales, especially in the sub-100 fs pumping. Effects of different pulse shapes, chirp in the ultrashort pulse, double pulses, and polarization dependence are some parameters that desire investigation in great detail.
4. Though many groups have focused their attention toward generating NPs using ULAL, very few groups[49, 111, 113] have attempted optimizing the NSs (left on targets) obtained with ULAL. Our group is directing our efforts toward applications from such NSs, especially for SERS studies of explosive materials.
5. Different, simple methods to overcome aggregation, agglomeration, oxidization of NPs, and oxidization of the NSs should be investigated further.
6. Usage of the plasmonic NSs created by ULAL for multiple times through simple cleaning mechanisms[258] need to be explored. In our case we could use the same substrate for recording SERS spectra of different molecules 2–3 times without any ambiguity in peak assignments.
7. Attention is required toward the application of ULAL-created NPs in anti-bacterial activities, bio-imaging, drug delivery, etc.

Over the last few years there have been a few pioneering works on ULAL by the Kabashin/Meunier group,[9, 37, 39, 114, 130, 134, 139, 140, 142, 157, 252–256] the Stratakis group,[47–49, 112, 121, 138, 257, 259–268] etc. Our group[269] is investigating the potential application of ULAL-generated metallic NPs for applications in the fields of

(a) explosives detection using SERS techniques,
(b) enhancements in luminescence,
(c) photonics, and
(d) biomedicine.

However, additional efforts from groups all over the world working on ULAL are indispensable to realizing the true potential of this technique.

Acknowledgments: The authors thank Professor Surya P. Tewari for his encouragement and support. The authors acknowledge the support of Ms. Bhavna Verma in compiling the references and tables. The authors also thank DRDO, India, for continued financial support.

References and Notes

1. T. H. Maiman, *Nature* 187, 493 **(1960)**.
2. S. Link and A. M. El-Syed, *Annu. Rev. Phys. Chem.* 54, 331 **(2003)**.
3. D. Perez, L. K. Beland, D. Deryng, L. J. Lewis, and M. Meunier, *Phys. Rev. B: Cond. Matter Mater. Phys.* 77, 014108 **(2008)**.
4. D. Perez and L. J. Lewis, *Phys. Rev B* 67, 184102 **(2003)**.
5. S. Eliezer, N. Eliaz, and E. Grossman, *Laser Part. Beams* 23, 15 **(2005)**.
6. S. Eliezer, N. Eliaz, and E. Grossman, *Phys. Rev. B* 69, 144119 **(2004)**.
7. J. Radziemski and D. A. Creamers, Laser Induced Plasma and Applications, Marcel Dekker, New York **(1989)**.
8. X. Huang and M. A. El-Sayed, *J. Adv. Res.* 1, 13 **(2010)**.
9. A. V. Kabshin, M. Meunier, C. Kingston, and J. T. Luong, *J. Phys. Chem. B* 107, 4527 **(2003)**.
10. H. Cui, P. Liu, and G. W. Yang, *Appl. Phys. Lett.* 89, 153124 **(2006)**.
11. M. Arruebo, R. F. Pacheco, M. R. Ibarra, and J. Santamaria, *Nanotoday* 2, 22 **(2007)**.
12. J. Prikulis, F. Svedberg, and M. Kall, *Nano Lett.* 4, 115 **(2004)**.
13. J. L. Elechiguerra, J. L. Burt, J. R. Moranes, A. C. Bragado, X. Gavo, H. H. Lara, and M. J. Yacaman, *J. Nano. Biotechn.* 3, 1 **(2005)**.
14. S. Petersen, J. Jakobi, and S. Barcikowski, *App. Surf. Sci.* 255, 5435 **(2009)**.
15. S. W. Tong, C. F. Zhang, C. Y. Jiang, G. Liu, Q. D. Ling, and E. T. Kan, *Chem. Phys. Lett.* 453, 73 **(2008)**.
16. A. I. Maaroof and G. B. Smith, *Thin Solid Films* 485, 198 **(2005)**.
17. M. Mishra, H. Kumar, and K. Tripathi, *Dig. J. Nanomat. Biostruc.* 3, 49 **(2008)**.
18. S. K. Das, S. U. Choi, W. Yu, and T. Pradeep, Nanofluids-Science and Technology, John Wiley & Sons, New York **(2007)**.
19. M. Raffi, F. Hussain, T. M. Bhatti, J. I. Akhter, A. Hameed, and M. M. Hasan, *J. Mater. Sci. Technol.* 24, 192 **(2008)**.

20. P. Jain, I. El-Sayed, and M. El-Sayed, *Nano Today* 2, 18 **(2007)**.
21. D. B. Sanchez, The surface plasmon resonance of supported noble metal nanoparticles: Characterization, laser tailoring, and SERS application, Ph.D. thesis. Madrid University **(2007)**.
22. P. K. Jain, X. Huang, I. H. El-Sayed, and M. El-Sayed, *Acc. Chem. Res.* 41, 1578 **(2008)**.
23. M. Shao, L. Lu, H. Wang, S. Luo, and D. D. Ma, *Microchim. Acta* 164, 157 **(2009)**.
24. I. Rianasari, L. Walder, M. Burchardt, I. Zawisza, and G. Wittstock, *Langmuir* 24, 9110 **(2008)**.
25. D. Batani, *Laser Part Beams* 28, 235 **(2010)**.
26. H. M. Smith and A. F. Turner, *Appl. Opt.* 4, 147 **(1965)**.
27. H. W. Kroto, J. R. Heath, S. C. O'Brien, R. F. Curl, and R. E. Smally, *Nature* 318, 162 **(1985)**.
28. A. M. Morales and C. M. Lieber, *Science* 279, 208 **(1998)**.
29. D. B. Chrisey, A. Pique, R. A. McGill, J. S. Horwitz, B. R. Ringeisen, D. M. Bubb, and P. K. Wu, *Chem. Rev.* 103, 553 **(2003)**.
30. H. B. Bebb and A. Gold, *Phys. Rev*. 143, 1 **(1966)**.
31. M. D. Perry, O. L. Landen, A. Szoke, and E. M. Campbell, *Phys. Rev. A* 37, 747 **(1988)**.
32. J. K. Chen and J. E. Beraun, *Numer. Heat Trans. A: Applns.* 40, 1 **(2001)**.
33. R. Fabbro, J. Fournier, P. Ballard, D. Devaux, and J. Virmont, *J. Appl. Phys*. 68, 775 **(1990)**.
34. T. Sakka, S. Ivanaga, Y. H. Ogata, A. Matsunawa, and T. Takemoto, *J. Chem. Phys.* 112, 8645 **(2000)**.
35. T. Sakka, K. Takatani, Y. H. Ogata, and M. Mabuchi, *J. Phys. D* 35, 65 **(2002)**.
36. C. J. Sajti, R. Sattari, B. N. Chichkov, and S. Barcikowski, *J. Phys. Chem. C* 114, 2421 **(2010)**.
37. P. Lorazo, L. J. Lewis, and M. Meunier, *Phys. Rev. Lett.* 91, 225502 **(2003)**.
38. S. Amoruso, G. Ausanio, A. C. Barone, R. Bruzzese, L. Gragnaniello, M. Vitiello, and X. Wang, *J. Phys. B: At. Mol. Opt. Phys.* 38, L329 **(2005)**.
39. P. Lorazo, L. J. Lewis, and M. Meunier, *Phys. Rev. B* 73, 134108 **(2006)**.
40. P. Balling and J. Schou, *Rep. Prog. Phys.* 76, 036502 **(2013)**.
41. N. G. Semaltianos, *Crit. Rev. Solid State Mater. Sci.* 35, 105 **(2013)**.
42. S. I. Dolgaev, A. A. Lyalin, A. V. Simakin, V. V. Voronov, and G. A. Shafeev, *App. Surf. Sci.* 109/110, 201 **(1997)**.
43. A. V. Simakin, V. V. Voronov, N. A. Kirichenko, and G. A. Shafeev, *Appl. Phys. A* 79, 1127 **(2004)**.
44. P. V. Kazakevich, A. V. Simakin, and G. A. Shafeev, *Quantum Electron.* 35, 831 **(2005)**.
45. T. S. Lau, G. Levi, F. Bozon-Verduraz, A. V. Petrovskaya, A. V. Simakin, and G. A. Shafeev, *App. Surf. Sci.* 254, 1236 **(2007)**.
46. P. V. Kazakevich, A. V. Simakin, V. V. Voronov, and G. A. Shafeev, *App. Surf. Sci.* 252, 4373 **(2006)**.
47. E. Stratakis, V. Zorba, M. Barberoglou, C. Fotakis, and G. A. Shafeev, *App. Surf. Sci.* 255, 5346 **(2009)**.
48. E. Stratakis, M. Barberoglou, C. Fotakis, G. Viau, C. Garcia, and G. A. Shafeev, *Opt. Exp.* 17, 12650 **(2009)**.
49. E. Stratakis, V. Zorba, M. Barberoglou, C. Fotakis, and G. A. Shafeev, *Nanotechnol.* 20, 105303 **(2009)**.
50. B. Kumar and R. K. Thareja, *J. Appl. Phys*. 108, 064906 **(2010)**.
51. N. Barsch, J. Jacobi, S. Weiler, and S. Barcikowski, *Nanotechnol.* 20, 445603 **(2009)**.
52. E. Messina, E. Cavallaro, A. Cacciola, R. Saija, F. Borghese, P. Denti, B. Fazio, C. D'Andrea, P. G. Gucciardi, M. A. Lati, M. Meneghetti, G. Compagnini, V. Amendola, and M. Marago, *J. Phys. Chem. C* 115, 5115 **(2011)**.
53. M. Potara, M. Baia, C. Farcau, and S. Astilean, *Nanotechnol.* 23, 055501 **(2012)**.
54. I. Sur, M. Altunbek, M. Kahraman, and M. Culha, *Nanotechnol.* 23**,** 357102 **(2012)**.
55. U. K. Parashar, V. Kumar, T. Bera, P. S. Saxena, G. Nath, S. K. Srivastava, R. Giri, and A. Srivastava, *Nanotechnol.* 22, 415104 **(2012)**.
56. P. P. Patil, D. M. Phase, S. A. Kulkarni, S. V. Ghaisas, S. K. Kulkarni, S. M. Kanetkar, S. B. Ogale, and V. G. Bhide, *Phys. Rev. Lett.* 58, 238 **(1987)**.
57. T. Sato, T. Lijima, M. Seki, and N. Inagaki, *J. Magn. Magn. Mater.* 65, 252 **(1987)**.
58. M. P. Pileni, *J. Phys. Chem*. 97, 6961 **(1993)**.
59. K. V. P. M. Shafi, Y. Koltypin, A. Gedanken, R. Prozorov, J. Balogh, J. Lendvai, and I. Felner, *J. Phys. Chem. B* 101, 6409 **(1997)**.
60. Q. Chen and Z. Zhang, *J. Appl. Phys. Lett.* 73, 3156 **(1998)**.
61. O. Yavas, *Phys. Rev. Lett.* 72, 2021 **(1994)**.
62. O. Yavas, *Appl. Phys. A*. 58, 407 **(1994)**.
63. H. K. Park, C. P. Grigoropoulos, C. C. Poon, and A. C. Tam, *Appl. Phys. Lett.* 68, 596 **(1996)**.
64. H. K. Park, X. Zhang, C. P. Grigoropoulos, C. C. Poon, and A. C. Tam, *J. Heat Transfer.* 118, 702 **(1996)**.
65. H. K. Park, D. Kim, C. P. Grigoropoulos, and A. C. Tam, *J. Appl. Phys.* 80, 4072 **(1996)**.
66. A. De Giacomo, M. Dell'Aglio, O. De Pascale, and M. Capitelli, *Spectrochim. Acta B* 62, 721 **(2007)**.
67. T. Tsuji, D. Thang, Y. Okazaki, M. Nakanishi, Y. Tsuboi, and M. Tsuji, *Appl. Surf. Sci.* 254, 5224 **(2008)**.
68. A. De Giacomo, A. De Bonis, M. Dell'Aglio, O. De Pascale, R. Gaudiuso, S. Orlando, A. Santagata, G. Senesi, F. Taccogna, and R. Teghil, *J. Phys. Chem. C* 115, 5123 **(2011)**.
69. L. Bethe, R. Fabro, P. Peyre, L. Tollier, and E. Bartnicki, *J. Appl. Phys.* 82, 2826 **(1997)**.
70. L. Bethe, A. Sollier, P. Peyre, R. Fabro, L. Tollier, and E. Bartnicki, *J. Appl. D: Appl. Phys.* 33, 2142 **(2000)**.
71. M. S. El-Shall, S. Li, T. Turkki, D. Graiver, U. C. Pernisz, and M. I. Baraton *J. Phys. Chem*. 99, 17805 **(1995)**.
72. S. I. Dolgaev, A. V. Simakin, V. V. Voronov, G. A. Shafeev, and F. Bozon-Verduraj, *App. Surf. Sci.* 186, 546 **(2002)**.
73. S. B. Wen, X. L. Mao, R. Grief, and R. E. Russo, *J. Appl. Phys*. 101, 023114 **(2007)**.
74. B. Kumar, D. Yadav, and R. K. Thareja, *J. Appl. Phys*. 110, 074903 **(2011)**.
75. S. Yang, Y. Jang, C. H. Kim, C. Hwang, J. Lee, S. Chae, S. Jung, and M. Choi, *Powder. Tech*. 197, 170**(2010)**.
76. C. Wu, X. Qiao, J. Chen, H. Wang, F. Tan, and S. Li, *Mater. Lett.* 60, 1828 **(2006)**.
77. H. Jia, J. Zeng, W. Song, J. An, and B. Zhao, *Thin Solid Films* 496, 281 **(2006)**.
78. P. Y. Lim, R. S. Liu, P. L. She, C. F. Hung, and H. C. Shih, *Chem. Phys. Lett.* 420, 304 **(2006)**.
79. M. J. Rosemary and T. Pradeep, *J. Colloids Inter. Sci.* 268, 81 **(2003)**.
80. M. S. Chargot, A. Gruszecka, A. Smolira, J. Cytawa, and L. Michalak, *Vacuum* 82, 1088 **(2008)**.
81. H. Huang and X. Yang, *Carbohyd. Res.* 339, 2627 **(2004)**.
82. J. Gu, W. Fan, A. Shimojima, and T. Okubo, *J. Solid State Chem*. 181, 957**(2008)**.
83. Y. Liu, L. Liu, and W. Chiu, *J. Phys. Chem. B* 108, 19237 **(2004)**.
84. H. Eerikainen and E. Kauppinen, *Int. J. Pharma.* 263, 69 **(2003)**.
85. K. L. McGilvray, M. R. Decan, D. Wang, and J. Scaiano, *J. Amer. Chem. Soc.* 128, 15980 **(2006)**.
86. M. Duocastella, J. M. Fernandez-Pradas, J. Dominguez, P. Serra, and J. L. Morenza, *Appl. Phys. A* 93, 941 **(2008)**.
87. S. Y. Yang and S. G. Kim, *Powder Technol*. 146, 185 **(2004)**.
88. N. S. Tabrizi, M. Ullmann, V. A. Vons, U. Lafont, and A. Schmidt-Ott, *J. Nanopart. Res.* 11, 315 **(2009)**.
89. S. Yang, W. Cai, H. Zhang, X. Xu, and H. Zeng, *J. Phys. Chem. C* 113, 19091 **(2009)**.

90. N. G. Semaltianos, S. Logothetidis, W. Perrie, S. Romani, R. J. Potter, M. Sharp, G. Dearden, and K. G. Watkins, *Appl. Phys. Lett.* 95, 033302 **(2009)**.
91. G. Compagnini, E. Messina, O. Puglisi, and V. Nicolosi, *Appl. Surf. Sci.* 254, 1007 **(2007)**.
92. C. He, T. Sasaki, Y. Shimizu, and N. Koshizaki, *Appl. Surf. Sci.* 254, 2196 **(2008)**.
93. G. X. Chen, M. H. Hong, B. Lan, Z. B. Wang, Y. F. Lu, and T. C. Chong, *Appl. Surf. Sci.* 228, 169 **(2004)**.
94. M. W. Murphy, P. G. Kim, X. Zhou, J. Zhou, M. Coulliard, G. A. Botton, and T. Sham, *J. Phys. Chem. C* 113, 4755 **(2009)**.
95. G. Compagnini, E. Messina, O. Puglisi, and R. S. Cataliotti, *Chem. Phys. Lett.* 457, 386 **(2008)**.
96. W. T. Nichols, T. Sasaki, and N. Koshizaki, *J. Appl. Phys.* 100, 114911 **(2006)**.
97. V. Amendola, and M. Meneghetti, *Phys. Chem. Chem. Phys.* 11, 3805 **(2009)**.
98. T. Tsuji, K. Iryo, Y. Nishimura, and M. Tsuji, *J. Photochem. Photobiol. A* 145, 201 **(2001)**.
99. Z. Yan, R. Bao, Y. Huang, A. Caruso, S. B. Qadri, C. Z. Dinu, and D. B. Chrisey, *J. Phys. Chem. C* 114, 3869 **(2010)**.
100. V. Amendola and M. Menghetti, *Phys. Chem. Chem. Phys*. 15, 3027 **(2013)**.
101. S. Z. Mortazavi, P. Parvin, A. Reyhani, A. N. Golikand, and S. Mirershadi, *J. Phys. Chem. C* 115, 5049 **(2011)**.
102. A. Schwenke, P. Wagener, S. Nolte, and S. Barcikowski, *Appl. Phys. A* 10, 77 **(2011)**.
103. C. Liu, A study of particle generation during laser ablation with applications, Doctoral Thesis, University of California, Berkeley **(2005)**, pp. 1–189.
104. T. Ctvrtnickova, L. Cabalin, J. Laserna, V. Kanicky, and G. Nicola, *Appl. Surf. Sci.* 255, 5329 **(2009)**.
105. D. Bauerle, Ultrashort-Pulse Laser Ablation in Laser Processing and Chemistry, 3rd edn., Springer-Verlag, New York **(2000)**, Chap. 13.
106. C. Momma, B. N. Chichkov, S. Nolte, F. Von Alvensleben, A. Tunnermann, H. Welling, and B. Wellegehausen, *Opt. Commun.* 129, 134 **(1996)**.
107. J. H. Yoo, S. H. Jeong, X. L. Mao, R. Grief, and R. E. Russo, *Appl. Phys. Lett.* 76, 783 **(2000)**.
108. K. Y. Niu, J. Yang, S. A. Kulinich, J. Sun, H. Li, and X. W. Du, *J. Am. Chem. Soc.* 132, 9814 **(2010)**.
109. G. W. Yang, *Prog. Mat. Sci.* 52, 648 **(2007)**.
110. T. Sasaki, Y. Shimizu, and N. Koshizaki, *J. Photochem. Photobiol. A Chem.* 186, 335 **(2006)**.
111. P. Liu, H. Cui, C. X. Wang, and G. W. Yang, *Phys. Chem. Chem. Phys.* 12, 3942 **(2010)**.
112. E. Stratakis, *Sci. Adv. Mater.* 4, 407 **(2012)**.
113. H. Zeng, X. Du, S. C. Singh, S. A. Kulinich, S. Yang, J. He, and W. Cai, *Adv. Funct. Mater.* 22, 1333 **(2012)**.
114. P. Lorazo, L. J. Lewis, and M. Meunier, *Phys. Rev. B* 73, 134 **(2006)**.
115. V. Kostrykin, M. Niessen, J. Jandeleit, W. Schulz, E. W. Kreutz, and R. Poprawe, *Proc. SPIE* 3343, 971 **(1998)**.
116. D. Von der Linde, K. Sokolowski-Tinten, and J. Barcikowski, *Appl. Surf. Sci.* 109–110, 1 **(1997)**.
117. B. N. Chichkov, C. Momma, S. Nolte, A. Alvensleben, and A. Tunnermann, *Appl. Phys. A* 63, 109 **(1996)**.
118. A. Moitello and R. Kelly, *Appl. Phys. A* 69, 67 **(1999)**.
119. Q. Lu, S. S. Mao, and R. E. Russoa, *Appl. Phys. Lett.* 80, 3072 **(2002)**.
120. P. T. Mannion, J. Magee, E. Coyne, G. M. O'Connor, and T. J. Glynn, *Appl. Surf. Sci.* 233, 275 **(2004)**.
121. E. V. Barmina, M. Barberoglu, V. Zorba, A. V. Simakin, E. Stratakis, C. Fotakis, and G. A. Shafeev, *Quantum Electron.* 39, 89 **(2009)**.
122. K. Leitz, B. Redlingshofer, Y. Reg, A. Otto, and M. Schmidt, *Phys. Proc.* 12, 230 **(2011)**.
123. S. Barcikowski, A. Menendez-Manjon, and B. Chichkov, *Appl. Phys. Lett.* 91, 083113 **(2007)**.
124. D. Riabinina, M. Chaker, and J. Margot, *Nanotechnol.* 23, 135603 **(2012)**.
125. L. V. Zhigilei, P. B. S. Kodali, and B. J. Garrison, *Chem. Phys. Lett.* 276, 269 **(1997)**.
126. L. V. Zhigilei, P. B. S. Kodali, and B. J. Garrison, *J. Phys. Chem. B* 101, 2028 **(1997)**.
127. L. V. Zhigilei and B. J. Garrison, *Mater. Res. Soc. Proc.* 538, 491 **(1999)**.
128. L. D. Landau, E. M. Lifshitz, and L. P. Pitaevskii, Electrodynamics of Continuous Media, Pergamon Press, Oxford **(1984)**.
129. K. A. Elsayed, H. Imam, M. A. Ahmed, and R. Ramadan, *Opt. Las. Tech.* 45, 495 **(2013)**.
130. A. V. Kabashin and M. Meunier, *J. Appl. Phys.* 94, 7941 **(2003)**.
131. J. B. Nielsen, J. M. Savolainen, M. S. Christensen, and P. Balling, *Appl. Phys. A* 101, 97 **(2010)**.
132. S. Barcikowski, A. Hahn, A. V. Kabashin, and B. N. Chichkov, *Appl. Phys. A* 87, 47 **(2007)**.
133. H. Kawasaki, *Nanotechnol. Rev.* 2, 5 **(2013)**.
134. J.-P. Sylvestre, A. V. Kabashin, E. Sacher, and M. Meunier, *Appl. Phys. A* 80, 753 **(2005)**.
135. R. M. Tilaki, A. Irajizad, and S. M. Mahdavi, *Appl. Phys. A* 84, 215 **(2006)**.
136. G. Krishna Podagatlapalli, S. Hamad, S. Sreedhar, S. P. Tewari, and S. Venugopal Rao, *Chem. Phys. Lett.* 530, 97 **(2012)**.
137. G. Krishna Podagatlapalli, S. Hamad, S. P. Tewari, S. Sreedhar, and S. Venugopal Rao, *J. Appl. Phys.* 113, 073106 **(2013)**.
138. E. B. Barmina, E. Stratakis, C. Fotakis, and G. A. Shafeev, *Quant. Electron.* 40, 1012 **(2010)**.
139. J. P. Sylvestre, S. Poulin, A. V. Kabashin, E. Sacher, M. Meunier, and J. H. T. Luong, *J. Phys. Chem. B* 108, 16864 **(2004)**.
140. É. Boulais, R. Lachaine, and M. Meunier, *J. Phys. Chem. C* 117, 9386 **(2013)**.
141. A. Barchanski, C. L. Sajti, C. Sehring, S. Petersen, and S. Barcikowski, *J. Laser Micro Nano Engg.* 6 **(2)**, 124 **(2009)**.
142. J. P. Sylvestre, A. V. Kabashin, E. Sacher, M. Meunier, and J. H. T. Luong, *J. Am. Chem. Soc.* 126, 7176 **(2004)**.
143. M. A. Sobhan, M. J. Withford, and E. M. Goldys, *Langmuir* 26, 3156 **(2010)**.
144. S. Petersen, A. Barchanski, U. Taylor, S. Klein, D. Rath, and S. Barcikowski, *J. Phys. Chem. C* 115, 5152 **(2011)**.
145. D. Tan, Y. Teng, Y. Liu, Y. Zhuang, and J. Qiu, *J. Nanopart. Res.* 13, 1183 **(2011)**.
146. N. G. Semaltianos, S. Logothetidis, W. Perrie, S. Romani, R. J. Potter, M. Sharp, P. French, G. Dearden, and K. G. Watkins, *Appl. Phys. A* 94, 641 **(2009)**.
147. A. Menendez-Manjon, J. Jakobi, K. Schwabe, J. K. Krauss, and S. Barcikowski, *J. Laser Micro Nano Engg.* 4, 95 **(2009)**.
148. N. Barsch, J. Jakobi, S. Weiler, and S. Barcikowski, *Nanotechnol.* 20, 445603 **(2009)**.
149. F. Bian, Y. C. Tian, R. Wang, H. X. Yang, H. X. Xu, S. Meng, and J. M. Zhao, *Nano Lett.* 11, 3251 **(2011)**.
150. E. V. Barmina, S. Lau Truong, F. Bozon-Verduraz, G. Levi, A. V. Simakin, and G. A. Shafeev, *Quant. Electron.* 40, 346 **(2010)**.
151. O. I. Eroshova, P. A. Perminov, S. V. Zabotnov, M. B. Gongalski, A. A. Ezhov, L. A. Golovan, and P. K. Kashkarov, *Cryst. Reports* 57, 831 **(2012)**.
152. P. G. Kuzmin, G. A. Shafeev, V. V. Bukin, S. V. Garnov, C. Farcau, R. Carles, B. W. Fonrose, V. Guieu, and G. Viau, *J. Phys. Chem. C* 114, 15266 **(2010)**.
153. T. Tsuji, M. Nakanishi, T. Mizuki, S. Ozono, M. Tsuji, and Y. Tsuboi, *Sci. Adv. Mat.* 4, 391 **(2012)**.
154. V. Amendola, S. Polizzi, and M. Meneghetti, *Sci. Adv. Mater.* 4, 497 **(2012)**.

155. H. Shi, C. Wang, Y. Zhou, K. Jin, and G. Yang, *J. Nanosci. Nanotechnol.* 12, 7896 (**2012**).
156. J. Liu, C. Liang, Z. Tian, S. Zhang, and G. Shao, *Sci. Reports* 3, 741 (**2013**).
157. A. V. Kabashin, F. Magny, and M. Meunier *J. Appl. Phys.* 101, 054311 (**2007**).
158. N. G. Semaltianos, S. Logothetidis, W. Perrie, S. Romani, R. J. Potter, S. P. Edwardson, P. French, M. Sharp, G. Dearden, and K. G. Watkins, *J. Nanopart. Res.* 12, 573 (**2010**).
159. V. Shukla, C. P. Singh, A. K. Srivastava, and K. S. Bindra, *J. Nanosci. Nanotechnol.* 12, 4644 (**2012**).
160. T. Salminen, J. Dahl, M. Tuominen, P. Laukkanen, E. Arola, and T. Niemi, *Opt. Mater. Express* 2, 799 (**2012**).
161. D. Garza, G. G. García, M. I. Mendivil Palma, D. Avellaneda, G. A. Castillo, T. K. Das Roy, B. Krishnan, and S. Shaji, *J. Mater. Sci.* 48, 6445 (**2013**).
162. P. Wagener, A. Schwenke, B. N. Chichkov, and S. Barcikowski *J. Phys. Chem. C* 114, 7618 (**2010**).
163. F. Abrinaei, M. J. Torkamany, M. R. Hantezadeh, and J. Sabbaghzadeh, *Sci. Adv. Mater.* 4, 501 (**2012**).
164. S. C. Singh, R. K. Swarnkar, and R. Gopal, *J. Nanosci. Nanotechnol.* 9, 5367 (**2009**).
165. E.-C. Chang, B.-C. Lin, P. Shen, and S.-Y. Chen, *J. Nanosci. Nanotechnol.* 12, 8337 (**2012**).
166. P. Moreno, C. Méndez, A. García, G. Torchia, D. Delgado, J. R. Vázquez De Aldana, L. Arias, and L. Roso, *J. Nanosci. Nanotechnol.* 6, 1961 (**2006**).
167. S. Lee, H. J. Jung, J. H. Shin, and M. Y. Choi, *J. Nanosci. Nanotechnol.* 12, 8900 (**2012**).
168. M. Fleischman, P. J. Hendra, and A. McQuillan, *J. Chem. Phys. Lett*. 26, 163 (**1974**).
169. D. L. Jeanmaire and R. P. V. Duyne, *Annu. Rev. Phys. Chem.* 84, 1 (**1977**).
170. M. G. Albrecht and J. A. Creighton, *J. Am. Chem. Soc.* 99, 5215 (**1977**).
171. H. J. Seki, *J. Electron Spectrosc. Relat. Phenom*. 39, 239 (**1986**).
172. M. Moskovits, *Rev. Mod. Phys*. 57, 783 (**1985**).
173. A. Crookell, M. Fleischmann, M. Hanniet, and P. J. Hendra, *Chem. Phys. Lett*. 149, 123 (**1988**).
174. D. B. Chase and B. A. Parkinson, *Appl. Spectrosc*. 42, 1186 (**1988**).
175. S. M. Angel, L. F. Katz, D. D. Archibald, and D. E. Hongis, *Appl. Spectrosc*. 43, 367 (**1989**).
176. K. Kniepp, *Exp. Tech. Phys.* 38, 3 (**1990**).
177. S. Nie and S. R. Emory, *Science* 275, 1102 (**1997**).
178. K. Kneipp, Y. Wang, H. Kniepp, L. T. Perelman, I. Itzkan, R. R. Dasari, and M. Feld, *Phys. Rev. Lett.* 78, 1667 (**1997**).
179. D. L. Stokes, D. Hueber, and T. Vo-Dinh, *Towards Single Molecule Detection with SERS Detection with SERS Detection Using Solid Substrates, 1998, Pittsburgh Conference*, New Orleans, LA, March (**1998**).
180. Y. Sun and Y. Xia, *Science* 298, 2176 (**2002**).
181. B. Wiley, Y. Sun, B. Mayers, and Y. Xia, *Chem. A. Eur. J.* 11, 454 (**2005**).
182. Y. Xia and N. J. Halas, *MRS Bull.* 30, 338 (**2005**).
183. C. L. Nehl, H. Liao, and J. H. Hafner, *Nano Lett.* 6, 683 (**2006**).
184. I. Lee, S. W. Han, and K. Kim, *J. Raman Spectrosc*. 32, 947 (**2001**).
185. K. Siskova, B. Vickova, P. Y. Turpin, and C. Fayet, *J. Phys. Chem. C* 112, 4435 (**2008**).
186. R. Buividas, P. R. Stoddart, and S. Juodkazis, *Ann. Phys. (Berlin)* 524, L5 (**2012**).
187. M. Prochazka, P. Mojzes, J. Stepanek, B. Vickova, and P. Turpin, *Anal. Chem.* 69, 5103 (**1997**).
188. M. Prochazka, J. Stepanek, B. Vickova, I. Srnova, and P. Maly, *J. Mol. Str.* 400, 213 (**1997**).
189. I. Srnova, M. Prochazka, B. Vickova, J. Stepanek, and P. Maly, *Langmuir* 14, 4666 (**1998**).
190. I. Lee, S. W. Han, and K. Kim, *J. Raman Spectrosc*. 32, 947 (**2001**).
191. M. Prochazka, J. Stepanek, P. Turpin, and J. Bok, *J. Chem. Phys. B* 106, 1543 (**2002**).
192. P. Smejkal, K. Siskova, B. Vickova, J. Pfleger, I. Sloufova, M. Slouf, and P. Mojzes, *Spect. Chim. Act. A* 59, 2321 (**2003**).
193. J. B. Zhang and Y. Fang, *Colloids and Surfaces A: Physicochem. Eng. Aspects* 266, 38 (**2005**).
194. N. Hajdukova, M. Prochazka, J. Stepanek, and M. Spirova, *Coll. Surf. A: Physicochem. Eng. Aspects* 301, 264 (**2007**).
195. J. Kneipp, X. Li, M. Sherwood, U. Panne, H. Kneipp, M. I. Stockman, and K. Kneipp, *Anal. Chem*. 80, 4247 (**2008**).
196. K. Siskova, B. Vickova, P. Turpin, A. Thorel, and M. Prochazka, *J. Phys. Chem. C* 115, 5404 (**2011**).
197. M. M. Mirinda, C. Gellini, and E. Giorgetti, *J. Phys. Chem. C* 115, 5021 (**2011**).
198. H. Guo, L. Ding, and Y. Mo, *J. Mol. Struct.* 991, 103 (**2011**).
199. Z. Luo, W. H. Woodward, and A. W. Castleman, *J. Raman Spectrosc*. 43, 1905 (**2012**).
200. C. Dong, Z. Yan, J. Kokx, D. B. Chrisey, and C. Z. Dinu, *Appl. Surf. Sci.* 258, 9218 (**2012**).
201. E. Giorgetti, M. M. Miranda, P. Marsili, D. Scarpellini, and F. Giammanco, *J. Nanopart. Res.* 14, 648 (**2012**).
202. E. Giorgetti, P. Marsili, P. Canton, M. M. Miranda, S. Caporali, and F. Giammanco, *J. Nanopart. Res.* 15, 1360 (**2013**).
203. W. Kaiser and A. Laubereau, Nonlinear Optics, edited by P. Harper and B. Wherrett, Academic, New York (**1977**).
204. P. N. Prasad and D. J. Williams, Introduction to Nonlinear Optical Effects in Molecules and Polymers, Wiley, New York (**1990**).
205. W. Koechner, Solid-State Laser Engineering, 3rd edn., Springer Ser. Opt. Sci., Springer, Berlin, Heildelberg (**1992**), Vol. 1.
206. G. I. Stegeman and A. Miller, Photonic Switching, edited by J. Michninter, Academic, Orlando (**1992**), Vol. 1, pp. 81–146.
207. D. K. Serkland, M. M. Fejer, R. L. Byer, and Y. Yamamoto, *Opt. Lett*. 20, 1649 (**1995**).
208. D. K. Serkland, P. Kumar, M. A. Arbore, and M. M. Fejer, *Opt. Lett*. 22, 1497 (**1997**).
209. Y. Guanjun, Z. Peng, Z. Dong, C. Zhang, C. Liangyao, and S. Qian, *Physica B* 393, 188 (**2007**).
210. H. Inouye, K. Tanaka, J. Tanahashi, T. Hattori, and H. Nakatsuka, *J. Appl. Phys.* 39, 5132 (**2000**).
211. J. F. Reintjes, Nonlinear Optical Parametric Processes in Liquids and Gases, Academic Press, New York (**1984**).
212. L. Francois, M. Mostafavi, J. Belloni, and J. A. Delaire, *Phys. Chem. Chem. Phys.* 3, 4965 (**2001**).
213. S. Qu, C. Du, Y. Song, Y. Wang, Y. Gao, S. Liu, Y. Li, and D. Zhu *Chem. Phys. Lett*. 356, 403 (**2002**).
214. M. Anija, J. Thomas, N. Singh, A. Nair, R. T. Tom, T. Pradeep, and R. Philip, *Chem. Phys. Lett*. 380, 223 (**2003**).
215. Y. Deng, Y. Sun, P. Wang, D. Zhang, X. Jiao, H. Ming, Q. Zhang, Y. Jiao, and X. Sun, *Curr. Appl. Phys*. 8, 13 (**2008**).
216. C. Torres-Torres, J. A. Reyes-Esqueda, J. C. Cheang-Wong, A. Crespo-Sosa, Rodríguez-L. Fernández, and A. Oliver, *J. Appl. Phys.* 104, 014306 (**2008**).
217. A. G. Luis, F. E. dos Santos, A. S. Gomes, C. B. de Araújo, P. L. R. Kassab, and G. H. Windson, *Appl. Phys. Lett*. 92, 141916 (**2008**).
218. R. Aleksandr, P. Bruno, S. Debrus, G. Rashid, A. Stepanov, C. Nurdogan, C. Buchal, and U. Sibel, *Appl. Opt.* 44, 2839 (**2005**).
219. J. M. Ballesteros, R. Serna, J. Solis, C. N. Afonso, A. K. Petford-Long, D. H. Osborne, and R. F. Haglund, Jr, *Appl. Phys. Lett.* 71, 2445 (**1997**).
220. R. del Coso and J. Solis, *J. Opt. Soc. Am. B* 21, 640 (**2004**).
221. R. A. Ganeev, A. I. Ryasnyansky, Sh. R. Kamalov, M. K. Kodirov, and T. Usmanov, *J. Phys. D: Appl. Phys.* 34, 1602 (**2001**).
222. S. Venugopal Rao, *J. Mod. Opt.* 58, 1024 (**2011**).
223. Y. Guillet, M. Rashidi-Huyeh, and B. Palpant, *Phys. Rev. B.* 79, 045410 (**2009**).

224. U. Kreibig and M. Vollmer, Optical Properties of Metal Clusters, Springer-Verlag, Berlin **(1995)**.
225. G. Ma, W. Sun, S. H. Tang, H. Zhang, Z, Shen, and S. Qian, *Opt. Lett.* 27, 1043**(2002)**.
226. Y. Guillet, M. Rashidi-Huyeh, D. Prota, and B. Palpant, *Gold Bull.* 41, 341 **(2008)**.
227. S. Venugopal Rao, T. S. Prashant, T. Sarma, P. K. Panda, D. Swain, and S. P. Tewari, *Chem. Phys. Lett.* 514, 98 **(2011)**.
228. D. Swain, P. T. Anusha, T. S. Prashant, S. P. Tewari, T. Sarma, P. K. Panda, and S. Venugopal Rao, *Appl. Phys. Lett*. 100, 141109 **(2012)**.
229. P. T. Anusha, D. Swain, S. Hamad, L. Giribabu, T. S. Prashant, S. P. Tewari, and S. Venugopal Rao, *J. Phys. Chem. C* 116, 17828 **(2012)**.
230. S. Hamad, S. P. Tewari, L. Giribabu, and S. Venugopal Rao, *J. Porphy. Phth.* 16 140 **(2012)**.
231. A. Nag, A. Kumar, P. P. Kiran, S. Chakraborty, G. R. Kumar, and D. D. Sarma, *J. Phys. Chem. C* 112, 8229 **(2008)**.
232. R. Philip, G. R. Kumar, N. Sandhyarani, and T. Pradeep, *Phys. Rev. B* 62 13160 **(2000)**.
233. P. Prem Kiran, B. N. S. Bhaktha, and D. Narayana Rao, *J. Appl. Phys.* 96, 6717 **(2004)**.
234. R. Sreeja, R. Reshmi, P. M. Aneesh, and M. K. Jayaraj, *Sci. Adv. Mater.* 4, 439 **(2012)**.
235. Y. Gao, X. Zhang, Y. Li, H. Liu, Y. Wang, Q. Chang, W. Jiao, and Y. Song, *Opt. Commun.* 51, 429 **(2005)**.
236. M. Samoc, A. Samoc, B. L. Davies, H. Reisch, and U. Scherf, *Opt. Lett.* 23, 1295 **(1998)**.
237. K. Kandasamy, K. D. Rao, R. Deshpande, P. N. Puntambekar, B. P. Singh, S. J. Shetty, and T. S. Srivastava, *Appl. Phys. B* 64, 479 **(1997)**.
238. K. P. Unnikrishnan, J. Thomas, V. P. N. Nampoori, and C. P. G. Vallabhan, *Opt. Commun*. 217, 269 **(2003)**.
239. M. Sheik-Bahae, A. A. Said, T. H. Wei, D. J. Hagan, and E. W. Van Stryland, *IEEE J. Quant. Electron.* 6, 760 **(1990)**.
240. B. Gu and W. Ji, *Opt. Exp.* 16, 10208 **(2008)**.
241. K. V. Saravanan, K. C. James Raju, M. G. Krishna, S. P. Tewari, and S. Venugopal Rao, *Appl. Phys. Lett.* 96, 232905 **(2010)**.
242. R. L. Sutherland, Handbook of Nonlinear Optics, Marcel Dekker, New York **(2003)**.
243. S. Dengler, C. Kubel, A. Schwenke, G. Ritt, and B. Eberle, *J. Opt.* 14, 075203 **(2012)**.
244. R. A. Ganeev, M. Baba, A. I. Ryasnyansky, M. Suzuki, and H. Kuroda, *Opt. Commun.* 240, 437 **(2004)**.
245. V. A. Karavanskii, A. V. Simakin, V. I. Krasovskii, and P. V. Ivanchenko, *Quan. Elect.* 34, 644 **(2004)**.
246. P. Jafarkhani, M. J. Torkamany, S. Dadras, A. Chehrghani, and J. Sabbaghzadeh, *Nanotechnology* 22, 235703 **(2011)**.
247. S. Alikhani, H. Tajalli, and E. Koushki, *Opt. Commun.* 286, 318 **(2013)**.
248. A. Nath, A. Das, L. Rangan, and A. Khare, *Sci. Adv. Mat.* 4, 106 **(2012)**.
249. S. Y. Liau, D. C. Read, W. J. Pugh, J. R. Furr, and A. D. Russel, *Lett. Appl. Microbiol.* 25, 279 **(1997)**.
250. S. Jadhav, A. Hussain, S. Devi, A. Kumar, S. Parveen, N. Gandham, L. H. Wieler, C. Ewers, and N. Ahmed, *PLoS One* 6, 18063 **(2011)**.
251. S. Petersen and S. Barcikowski, *Adv. Funct. Mater.* 19, 1167 **(2009)**.
252. S. Besner, A. V. Kabashin, and M. Meunier, *Appl. Phys. A* 88, 269 **(2007)**.
253. S. Besner, A. V. Kabashin, and M. Meunier, *Appl. Phys. Lett.* 89, 233122 **(2006)**.
254. S. Besner, A. V. Kabashin, F. M. Winnik, and M. Meunier, *J. Phys. Chem. C* 113, 9526 **(2009)**.
255. S. Besner, A. V. Kabashin, F. M. Winnik, and M. Meunier, *Appl. Phys. A* 93, 955 **(2008)**.
256. A. V. Kabashin and M. Meunier, *J. Phys.: Conf. Ser.* 59, 354 **(2007)**.
257. C. Rehbock, V. Merk, L. Gamrad, R. Streubel, and S. Barcikowski, *Phys. Chem. Chem. Phys.* 15, 3057 **(2013)**.
258. X.-M. Lin, Y. Cui, Y.-H. Xu, B. Ren, and Z.-Q. Tian, *Anal. Bioanal. Chem.* 394, 1729 **(2009)**.
259. A. Ranella, M. Barberoglou, S. Bakogianni, C. Fotakis, and E. Stratakis, *Acta Biomater.* 6, 2711 **(2010)**.
260. E. V. Barmina, A. A. Serkov, E. Stratakis, C. Fotakis, V. N. Stolyarov, I. N. Stolyarov, and G. A. Shafeev, *Appl. Phys. A* 106, 1 **(2012)**.
261. E. Stratakis, A. Ranella, and C. Fotakis, *Biomicrofluidics* 5, 013411 **(2011)**.
262. E. V. Barmina, E. Stratakis, M. Barberoglu, V. N. Stolyarov, I. N. Stolyarov, C. Fotakis, and G. A. Shafeev, *Appl. Surf. Sci.* 258, 5898 **(2012)**.
263. P. Wagener, S. Ibrahumkutty, A. Menzel, A. Plech, and S. Barcikowski, *Phys. Chem. Chem. Phys.* 15, 3068 **(2013)**.
264. A. De Giacomo, M. Dell'Aglio, A. Santagata, R. Gaudiuso, O. De Pascale, P. Wagener, G. C. Messina, G. Compagnini, and S. Barcikowski, *Phys. Chem. Chem. Phys.* 15, 3083 **(2013)**.
265. S. Barcikowski, A. Hahn, and B. N. Chichkov, *J. Laser Applns.* 19, 65 **(2007)**.
266. S. Ibrahumkutty, P. Wagener, A. Menzel, A. Plech, and S. Barcikowski, *Appl. Phys. Lett.* 101, 103104 **(2012)**.
267. A. Meńendez-Manjon and S. Barcikowski, *Appl. Surf. Sci.* 257, 4285 **(2011)**.
268. J. Jakobi, A. Meńendez-Manjon, V. S. K. Chakravadhanula, L. Kienle, P. Wagener, and S. Barcikowski, *Nanotechnol.* 22, 145601 **(2011)**.
269. S. Hamad, G. Krishna Podagatlapalli, Surya P. Tewari, and S. Venugopal Rao, *J. Phys. D: Appl. Phys.* 46, 485501 **(2013)**.

Received: 3 August 2013. Accepted: 11 November 2013.